



Calhoun: The NPS Institutional Archive
DSpace Repository

Theses and Dissertations

1. Thesis and Dissertation Collection, all items

1956

Optimum prediction for a torque saturating servo

Gay, William W.; McCord, Wayne S.

University of Michigan

<http://hdl.handle.net/10945/14479>

Downloaded from NPS Archive: Calhoun



Calhoun is the Naval Postgraduate School's public access digital repository for research materials and institutional publications created by the NPS community. Calhoun is named for Professor of Mathematics Guy K. Calhoun, NPS's first appointed -- and published -- scholarly author.

Dudley Knox Library / Naval Postgraduate School
411 Dyer Road / 1 University Circle
Monterey, California USA 93943

<http://www.nps.edu/library>

OPTIMUM PREDICTION
FOR A TORQUE SATURATING
SERVO

WILLIAM W. GAY.
WAYNE S. McCORD

1956

Library
U. S. Naval Postgraduate School
Monterey, California

OPTIMUM PREDICTION FOR A
TORQUE SATURATING SERVO

by

William W. Gay

and

Wayne S. McCord

May 1956

TABLE OF CONTENTS

Library
U. S. Naval Postgraduate School
Monterey, California

Table of Contents	ii
Summary	iii
Symbols	v
Introduction	1
Simulation	2
Procedure	2
Results and Discussion	6
Application to an Instrument Servo	9
Equipment	9
Procedure	11
Results and Discussion	13
Conclusions	15
References	49
Appendix I - Optimum Switching Criteria	I-1
Appendix II - The Function Generator	II-1
Appendix III - Magnetic Amplifier Characteristics and Compensation	III-1

OPTIMUM PREDICTION FOR A TORQUE SATURATING SERVO

SUMMARY

This study was made to examine the use of a particular type of nonlinear control for a torque saturating second order servomechanism. The control involves mechanization with diode limiters and operational amplifiers of a torque switching curve in the phase plane of error and error rate, with a region of linear operation about the curve. The switching curve is shaped to give prediction for optimum time response and essentially no overshoot for step and ramp inputs.

The results of simulation on an electronic differential analyzer show a large reduction in both response time and overshoot for a servo with prediction as compared to the same servo with proportional plus error rate control.

The introduction of an approximation to the true switching curve and moderate amounts of friction had little influence on the operation of the prediction control. The shape of the curve could be altered to optimize for any particular combination of Coulomb or viscous friction coefficients; however, the improvement was small.

The application of the nonlinear control to an instrument servo consisting

of a 400 cycle per second, two-phase motor coupled directly to a one-turn film potentiometer substantiated the results obtained by simulation. The characteristics of the signal from the film potentiometer permitted use of an approximate differentiator in the control circuit. With this system a resolution of one part in 40,000 and a response time of 0.06 seconds to a half-turn step input were obtained.

SYMBOLS

C	Coulomb friction torque, lb. -ft.
C_e	error rate coefficient, $2\mathcal{J}/\omega_n$
e	control voltage
f	viscous friction coefficient, lb. -ft. -sec.
i	subscript meaning input
I	moment of inertia, slug-ft. ²
K	a constant, $\mu/2T_m$ or $\mu/2(T_m + C)$
m	$\sqrt{2f^2/IT_m}$, subscript meaning maximum
o	subscript meaning output
R	resistance, megohms unless otherwise specified
t	time, seconds
T	torque, lb. -ft.
v	voltage
x	$\sqrt{1/2T_m} \dot{\epsilon}$
ϵ	error, $\theta_i - \theta_o$, radians
ϵ_1	error to torque-saturate the servo, T_m/μ
$\dot{\epsilon}$	$d\epsilon/dt$
$\dot{\epsilon}_m$	maximum error rate, T_m/f
$\ddot{\epsilon}$	$d^2\epsilon/dt^2$
\mathcal{J}	damping ratio
θ	angular position, radians
μ	gain constant
π	3.14159

τ	time constant, I/f
ω_n	undamped natural frequency, $\omega_n^2 = \mu/I$
Ω	input angular frequency

OPTIMUM PREDICTION FOR A TORQUE SATURATING SERVO

INTRODUCTION

The design of the controller for a servomechanism is based to a large extent on the particular type of input function and the requirements on the servo such as response time, accuracy, and amount of overshoot. Linear methods of control are extensively used as they are easy to implement and analyze. Since linear control does not necessarily represent the optimum design in most cases, considerable work has been done recently to improve performance by nonlinear techniques.

One such technique involves use of prediction or switching circuits intended to give optimum time response and limitation of overshoot for step or ramp inputs or combinations of the two. Previous investigations of methods of control, using some measure of prediction include nonlinear damping functions $(B, C)^*$, prediction with relay servos (C, D) and multiple mode techniques (E) .

Of particular interest is the work of Hopkin (F) , whose approach to prediction is very similar to that in this study although mechanized in a different manner.

It is the purpose of this investigation to extend previous work by the

* Parenthetical superscripts refer to references.

examination of use of a particular type of prediction in the control of a torque saturating, second order servomechanism. The basic theory was originally developed by L. L. Rauch and R. M. Howe^(A) and is summarized in Appendix I. This study develops a method of implementation of the theory for simulation in several phases and application to a specific instrument servo.

This investigation was undertaken by William W. Gay and Wayne S. McCord as a joint thesis project to satisfy, in part, the requirements for a Master of Science Degree in Aeronautical Engineering at the University of Michigan.

SIMULATION

Simulation was undertaken to obtain computer solutions to theoretical equations of the servo problem under study. These solutions were obtained for several variations of the servo setup in order to make a series of comparisons.

PROCEDURE

The servo setups considered were those of:

1. A servo using proportional and error rate control without prediction.
2. A servo using proportional and error rate control with prediction.
3. The same servo as in #2 but with an approximate prediction curve.
 - a. No friction.
 - b. With Coulomb and/or viscous friction
(but no compensation for friction in the prediction curve).
 - c. With Coulomb and/or viscous friction
(with compensation for Coulomb or viscous friction).
4. The same servo as in #3, a., but with approximate differentiation of error to obtain error rate.

The first point considered in the simulation was to show the improvement in response time and reduction of overshoot by adding prediction to a servo with proportional plus error rate control.

The equation for a torque-saturating, frictionless servo employing proportional and error rate control is

$$I \ddot{\theta}_o = \mu [\epsilon + C_e \dot{\epsilon}]_{sat} \pm \frac{T_m}{\mu}$$

To adapt the equation to the computer for solution, it was time scaled by the undamped natural frequency, ω_n , and magnitude scaled by the error required for torque saturation, ϵ_λ . These quantities are defined as

$$\omega_n^2 = \frac{\mu}{I}$$

$$\epsilon_\lambda = \frac{T_m}{\mu}$$

$$\text{Also, } C_e = \frac{2 \gamma}{\omega_n}$$

where γ is the damping ratio. The equation can then be written

$$\frac{\ddot{\epsilon}}{\omega_n^2} = [\epsilon + 2 \gamma \frac{\dot{\epsilon}}{\omega_n}]_{sat} \pm \epsilon_\lambda$$

The arbitrary values of parameters chosen were $\omega_n = 1$, $\gamma = 0.5$, and $\epsilon_\lambda = 0.025$, where unity was represented by 100 volts in the computer. The solutions were then presented in dimensionless form as $\dot{\epsilon}/\omega_n$ versus $\epsilon/\epsilon_\lambda$ in the phase plane and $\epsilon/\epsilon_\lambda$ versus $\omega_n t$ in the time plots. Figure 1 shows the computer circuit for solution of this equation.

The effect of torque saturation was obtained by limiting with operational amplifiers. The output stage of each amplifier was a cathode follower. When

the outputs of two amplifiers were connected in parallel, the more positive signal determined the output of the pair. Thus by introducing a constant positive voltage into the input of one of the paralleled amplifiers, the output of the pair was limited in the negative direction. By using two such pairs in cascade, both plus and minus limiting was obtained.

The addition of prediction modifies the equation of motion of the above servo to the form developed in Appendix I.

$$I\ddot{\theta}_o = \mu \left[\epsilon + (C_e \dot{\epsilon})_{sat} \pm \frac{T_m}{J_m} + \frac{J}{2T_m} |\dot{\epsilon}| \dot{\epsilon} \right]_{sat} \pm \frac{T_m}{J_m}$$

The method for adapting this equation to a suitable form for computer solution is identical to the procedure used previously with the result

$$\frac{\ddot{\theta}_o}{\omega_n^2} = \left[\epsilon + (Z Y \frac{\dot{\epsilon}}{\omega_n})_{sat} \pm \frac{J}{2J_n} \left| \frac{\dot{\epsilon}}{\omega_n} \right| \frac{\dot{\epsilon}}{\omega_n} \right]_{sat} \pm \epsilon_f$$

This equation was actually solved by two different computer circuits. Figure 2 shows the computer circuit for exact solution. A servo multiplier was used to form the product $\left| \frac{\dot{\epsilon}}{\omega_n} \right| \frac{\dot{\epsilon}}{\omega_n}$.

The computer circuit in Figure 3 was also used to solve this equation. In this case, a diode limiter network at the input to an operational amplifier generated an approximation to the prediction curve. The limiting network and approximate prediction curve for this case with no friction are shown in Figure 5. The diode networks used in this and subsequent computer circuits were developed by the methods presented in Appendix II.

Friction was introduced into the servo problem with no change in the prediction curve.

With Coulomb or viscous friction, the equations, when adapted for computer

solution, became respectively

$$\ddot{\theta}_n = \left[\epsilon + (2\tau \frac{\dot{\epsilon}}{\omega_n})_{sat \pm \epsilon_n} + \frac{1}{2\epsilon_n} \left| \frac{\dot{\epsilon}}{\omega_n} \right| \frac{\dot{\epsilon}}{\omega_n} \right]_{sat \pm \epsilon_n} \pm \frac{C}{\mu}$$

$$\ddot{\theta}_n + \left(\frac{1}{\tau \omega_n} \right) \dot{\theta}_n = \left[\epsilon + (2\tau \frac{\dot{\epsilon}}{\omega_n})_{sat \pm \epsilon_n} + \frac{1}{2\epsilon_n} \left| \frac{\dot{\epsilon}}{\omega_n} \right| \frac{\dot{\epsilon}}{\omega_n} \right]_{sat \pm \epsilon_n}$$

where $\tau = 1/f$ is the servo time constant, and C is the Coulomb friction torque.

The effect of Coulomb friction was introduced in the computer as a change in torque saturation levels depending on the sign of $\dot{\theta}_0$. Viscous friction was introduced in the computer as a feedback in the $\dot{\theta}_0/\omega_n$ integrator. The circuit additions are shown in Figure 3 in dashed lines.

Next, compensation for Coulomb and viscous friction effects was introduced by changing the approximate prediction function.

When the prediction is optimized for a specific Coulomb friction, the equation for the predictor servo, when adapted for computer solution becomes

$$\ddot{\theta}_n = \left[\epsilon + (2\tau \frac{\dot{\epsilon}}{\omega_n})_{sat \pm \epsilon_n} + \frac{1}{2(\tau_n + C)} \left| \frac{\dot{\epsilon}}{\omega_n} \right| \frac{\dot{\epsilon}}{\omega_n} \right]_{sat \pm \epsilon_n} \pm \frac{C}{\mu}$$

The diode limiting network and approximate prediction curve designed to include compensation for Coulomb friction of $C/T_m = 0.3$ were unchanged from Figure 5.

The only requirement was to multiply the coefficient of $\dot{\epsilon}/\omega_n$ by the factor $\sqrt{\frac{1}{1 + C/T_m}}$.

When the prediction curve is optimized for a specific viscous friction, the equation, when adapted for computer solution becomes

$$\frac{\ddot{\theta}}{\omega_n^2} + \left(\frac{1}{\tau\omega_n}\right) \frac{\dot{\theta}}{\omega_n} = \left[\epsilon + (2\tau\frac{\dot{\epsilon}}{\omega_n})_{sat} \pm \epsilon_p \right. \\ \left. \pm (\tau\omega_n)^2 \frac{T_m}{J_m} \left\{ \ln \left[1 + \left(\frac{1}{\tau\omega_n}\right) \left(\frac{J_m}{T_m}\right) \left(\frac{\dot{\epsilon}}{\omega_n}\right) \right] - \left(\frac{1}{\tau\omega_n}\right) \left(\frac{J_m}{T_m}\right) \left(\frac{\dot{\epsilon}}{\omega_n}\right) \right\} \right]_{sat} \pm \epsilon_p$$

The diode limiting networks and approximate prediction curve compensating for viscous friction are shown in Figure 6 for $\tau\omega_n = 10$ and $\tau\omega_n = 8.95$.

Approximate differentiation was introduced only for the servo with no friction. The computer equation developed previously still applies. The computer setup and approximate differentiation circuit are shown in Figure 4.

RESULTS AND DISCUSSION

The results of the simulation study were derived entirely from the phase plane and time plots for the various conditions outlined previously. Since some effects are more apparent in one representation than the other, certain solutions were recorded in the phase plane and also as a time function. Complete duplication of phase plane and time plots was not attempted. The solutions were grouped so a comparison of certain methods of control could be made to determine the answers to five questions.

1. Does the use of this type of prediction materially improve the performance of a servo system?
2. Does an approximation to the prediction curve materially degrade servo performance?
3. How much does friction affect servo performance when prediction is used?

4. Does compensation for friction effects materially improve the servo performance?

5. Is approximate differentiation of error to obtain error rate feasible for this system?

A measure of the improvement in performance due to prediction is available from the solutions in Figures 7 through 13. For small step inputs the servo with prediction shows no reduction in the size of the overshoot or response time. However, as the size of the input was increased, the improvement became very pronounced. For a step of $\epsilon/\epsilon_x = 32$, the overshoot was reduced by about 95% and response time by 65%.

Of interest in this comparison are the responses, in Figures 14 through 16, of the servo with and without prediction to sine wave inputs. Although there is no particular significance to this type of response and the prediction was not optimized for it, the improvement was still evident. For the highest frequency input, the servo with prediction could follow the signal, while the servo without prediction developed a divergent error. This condition was shown in Figure 16 where the input frequency was 1/3 of the servo natural frequency and the ratio of the maximum acceleration of the input to the maximum acceleration of the servo was 8/9.

Typical solutions of the servo response using an approximation to the prediction curve are presented in Figures 17 (a) and (b) and 18. A comparison of these solutions to those in Figures 9 (a), 8 (a) and 12 respectively shows no perceptible difference. Since the operation of the system with this five-segment approximation was satisfactory, no solutions were made using a more exact approximation to the true switching curve. All the remaining solutions were obtained with this method of generating the prediction curve.

The selection of friction coefficients to demonstrate the effects of friction was somewhat arbitrary. The Coulomb friction to torque ratio corresponds to that specified for the servo later tested. Since the viscous friction of this system was small, corresponding to $\tau \omega_n = 100$, additional values of viscous friction were selected to emphasize the effect. The change in the response with either type of friction is most evident in the phase plane plots of Figures 19 and 20. This change appears as a considerable reduction in error rate, but it may be observed in the error versus time plots in Figures 21 and 22 that the actual increase in response time was small even for these large amounts of friction. It may be noted that when either type of friction was present the solution path lay somewhat within the linear region during deceleration, indicating that less than maximum torque was being used.

In view of the fact that friction has the effect of slowing servo response to some extent, it was necessary to determine if response could be improved by changing the prediction curve to permit utilization of maximum torque during deceleration.

Figures 23 and 24 show phase plane and time plots where the prediction curve was altered to take into account the presence of Coulomb friction. These plots may be compared to those in Figures 20 and 22 for the same conditions but with prediction calculated for no friction. A very minor improvement in response time was obtained by altering the prediction curve to compensate for Coulomb friction. More improvement was noted as size of the step was increased.

In considering the various runs in Figures 25 through 29 it immediately becomes obvious that little improvement in servo time response was obtained when the prediction curve was altered to take into account viscous friction. It may be

noted that Figures 25 and 26 show a case where no velocity saturation due to viscous friction occurred. Figures 27 through 29 show a case where velocity saturation was approached.

It may be said that prediction to include either type of friction effects is feasible but offers little advantage.

By examining Figure 30 it is apparent that approximate differentiation was satisfactory in that the phase plane plot appears quite similar to phase plane plots where the true value for error rate was used in computation.

Stability was a problem in the simulation, however, and would presumably be a serious problem in application. The time constants of the differentiating circuit for the simulation were selected in order to avoid oscillation.

APPLICATION TO AN INSTRUMENT SERVOMECHANISM

A physical system was constructed to demonstrate in practice the use of approximate differentiation and an approximate prediction curve similar to the one examined in the simulation.

EQUIPMENT

Motor. The servo motor was a two phase, 400 cycle per second, 115 volt Transicoil motor, type 18M. Rated stall torque - 3.0 oz.-in., moment of inertia - 0.0197 oz.-in.², stall watts per phase - 18 watts, Coulomb friction - 0.10 oz.-in., coefficient of viscous friction - 0.00285 oz.-in.-sec.

Potentiometer. Feedback voltage was obtained from a three section, continuous film potentiometer, model number 205, made by Computer Instruments Corporation, Resistance - 50,000 ohms per section. Total moment of inertia -

0.164 oz.-in.², total Coulomb friction - 0.895 oz.-in., total viscous friction - negligible.

Diode limiting circuits. This is the circuit described in Appendix II, Figure II-3.

Compensation and control circuits. The compensation and control circuits utilized the operational amplifiers of a standard analog computer.

Power Amplifier. Two different power amplifiers were used to drive the control phase of the motor. One was a 115 volt, 400 cycle per second, push-pull, magnetic amplifier, Magnetic Amplifiers Inc. Model MA 41501-CY.

The other amplifier was an A. C. electronic amplifier used in conjunction with a 400 cycle per second chopper to convert the D. C. control signal to a 400 cycle per second A. C. signal. This amplifier was originally designed as a 60 cycle per second servo amplifier and was adapted for use with this system.

The choice of equipment was governed primarily by the requirements of the control circuits, specifically the differentiator. The film potentiometer was selected in preference to a wire wound potentiometer because the signal obtained had less noise and better resolution. The wire-to-wire discontinuities of a wire wound potentiometer would have introduced large errors in the differentiated signal and contributed to the instability of the differentiating amplifier.

The motor was selected from those available on the basis of largest torque to inertia ratio. It was coupled directly to the potentiometer to eliminate the backlash and binding problems of gear trains. Although the motor-to-load inertia balance was not good, the acceleration loss due to direct coupling was small. The best gear ratio, if used, would have been about three to one.

Initially a magnetic amplifier was chosen for power amplification because

of simplicity and reliability. The severe bandwidth limitations were alleviated somewhat by compensation as described in Appendix III so that the response was flat out to 200 cycles per second. However, the response time of the servo was short enough that the 200 cycles per second bandwidth still represented a limitation which appeared as a time delay. When the system gain was increased to obtain reasonable resolution, the time lag in the magnetic amplifier sustained oscillations of the servo at a frequency of 80 to 120 cycles per second, depending upon the particular gain setting. The oscillations were similar to those that would be experienced by an identical bang-bang servo with a fixed switching delay of about 5 milliseconds. This time delay was verified by observation of the control and output signals of the magnetic amplifier on a dual beam oscilloscope. The electronic amplifier and chopper were substituted when operation with the magnetic amplifier did not produce the potential resolution or tracking performance of the servo.

PROCEDURE

The servo was operated to obtain a comparison of the system with proportional control, proportional plus error rate control and proportional plus error rate control with prediction. The comparison was made by observing only the step response, and no attempt was made to analyze the servo completely. As an item of interest, the velocity lag and constant input errors were measured.

The basic servo circuit diagram is shown in Figure 31. Appropriate modifications to this basic circuit were made to obtain the particular types of control. The servo loop gain was adjusted to the highest possible value consistent with stable operation. If the gain was further increased, the servo went into a very

low amplitude oscillation at about 160 cycles per second.

The time constants of the approximate differentiating circuit were determined empirically with a view toward limiting noise and high frequency oscillations yet retaining sufficient bandwidth for good operation. The time constant of 0.0005 seconds corresponds to 319 cycles or roughly twice the maximum response frequency of the servo. The basic differentiating circuit, with constant gain at high frequencies (within the capabilities of the operational amplifier), passed too much noise, so the additional capacitor was added in the feedback to give a -6 db per octave roll off of gain for frequencies above 319 cycles per second.

The approximations in differentiation modified the error rate signal such that the amplitude was not increased in proportion to the frequency as prescribed for exact differentiation. Some compensation for the resulting loss of gain was made in the next amplification stage where the product $\sqrt{\frac{\pi I}{2(T_m + C)}} \dot{e}$ was formed. In place of using a calculated gain of 3.16 in this amplifier, the gain was increased to 4. The value of 4 was determined empirically for satisfactory servo response. The factor π in $\sqrt{\frac{\pi I}{2(T_m + C)}}$ is the scale factor between the output measured in radians and computer units, where 100 volts represents unity in the computer.

Photographs of the cathode ray oscilloscope presentation were made for phase plane and error versus time response of the servo to a 100 volt peak-to-peak 3 cycle per second square wave input. Similar photographs were made of the error versus time response for a 10 volt peak-to-peak 5 cycle per second square wave input.

The constant input error was measured by disturbing the servo slightly and noting the maximum error when the output had come to rest. The error

was actually measured on a voltmeter having a full scale deflection of 0.1 volt.

The velocity lag was measured in a manner similar to the constant input error. The effect of a ramp input was produced by a 0.5 cycle per second triangular wave. The frequency of the triangular wave was low enough that the transient effects damped sufficiently to permit accurate measurement of the velocity lag.

RESULTS AND DISCUSSION

Qualitatively the performance of the servo corresponded closely to results of the simulation. Although specific performance of the servo was not an objective, the response time, ability to track a slowly varying signal and the resolution approached closely the potential capability of the system.

The measured value of maximum steady state error was ± 0.005 volts. The terminal voltages on the potentiometer were ± 100 volts with the center-tap grounded. Based on this reference voltage range of 200 volts, the maximum steady state error corresponds to resolution of at least one part in 40,000.

From the maximum steady state error, an approximation to the width of the linear region ($2\epsilon_L$) may be calculated. The Coulomb friction to rated torque ratio was 0.33. However, actual measurement of the stall torque of the motor as driven by the electronic amplifier was about 2 oz.-in., giving an actual friction to torque ratio of about 0.5. Using this ratio, the linear region was calculated to be in the order of 0.02 volts.

Among the factors contributing to the low value of torque were poor output waveform from the electronic amplifier and somewhat less than 90° phase shift between the two motor phase voltages.

The photographs of the oscilloscope presentations of the phase plane and error versus time responses are shown in Figure 32. The system using proportional control exhibited a series of fairly large overshoots and long response time. Addition of error rate control ($\gamma = 0.5$) reduced the size and number of overshoots and response time. Furthermore, addition of prediction essentially eliminated overshoot and very substantially reduced response time. As expected, the improvement due to prediction was much more pronounced for the larger steps. As an example, for the 100 volt step input the response times were 0.17, 0.13 and 0.06 seconds for the three types of control.

Measurements were made of velocity lag and are recorded in Table I.

TABLE I
VELOCITY LAG (All Types of Control)

\dot{e}_i (volts/sec.)	Error (volts)
0.5	0.01
1	0.014
2	0.02
5	0.03
10	0.04
20	0.06
40	0.076
80	0.08
120	0.10
160	0.13

Since the rotation of the motor was limited to at most one revolution, the velocity never exceeded 20% of the maximum motor velocity. Within this range, the viscous friction effects of the servo were negligible. For practical considerations, this fact plus the very narrow linear region makes the response of the servo to a step input of several volts very similar to that of a bang-bang servo

with only Coulomb damping.

The response of the servo with proportional control to the 100 volt step input exhibits a ratio of successive overshoots of about 0.4. Calculations using this ratio for a theoretical bang-bang servo with Coulomb damping indicate a Coulomb friction to torque ratio of 0.43, which checks closely with the ratio of the measured values, 0.5.

The response of the servo with prediction can also be compared to the theoretical response of a corresponding bang-bang servo. Again for the 100 volt step input, the observed response time was 0.06 seconds which compares to a computed time of 0.063 seconds.

CONCLUSIONS

Based on the results obtained in the simulation and in application to the instrument servo it is concluded that:

1. Use of prediction reduces response time and overshoot, particularly for large step and ramp inputs.
2. Use of prediction improves transient response of the servo for arbitrary input signals, such as a sine wave input, even though the prediction was optimized only for step and ramp inputs.
3. Use of simple approximations to the exact prediction curve does not degrade performance.
4. Modification of the prediction curve to optimize for friction effects was possible but little improvement was achieved over the prediction curve optimized for no friction.
5. Noise level in the output signal from the film potentiometer was low,

thus permitting differentiation with an operational amplifier to obtain approximate error rate signal.

6. Resolution of the film potentiometer and direct coupling permitted a degree of control sufficient to give servo resolution of one part in 40,000.
7. For high loop gains the region of linear operation was very narrow, hence, the system acted much like a bang-bang servo with Coulomb damping.

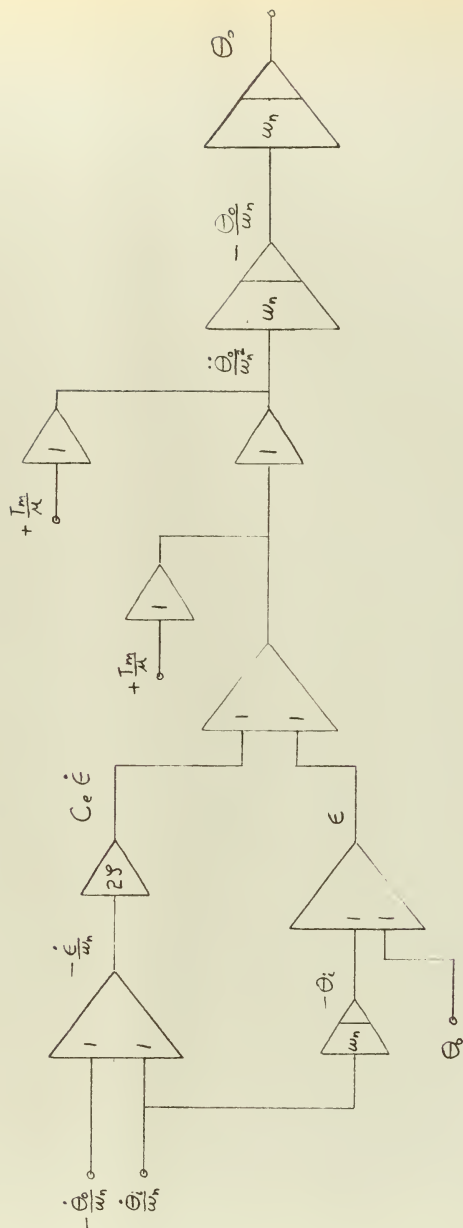


FIGURE 1 — Computer Circuit for a Frictionless Servo
with Proportional and Error Rate Control



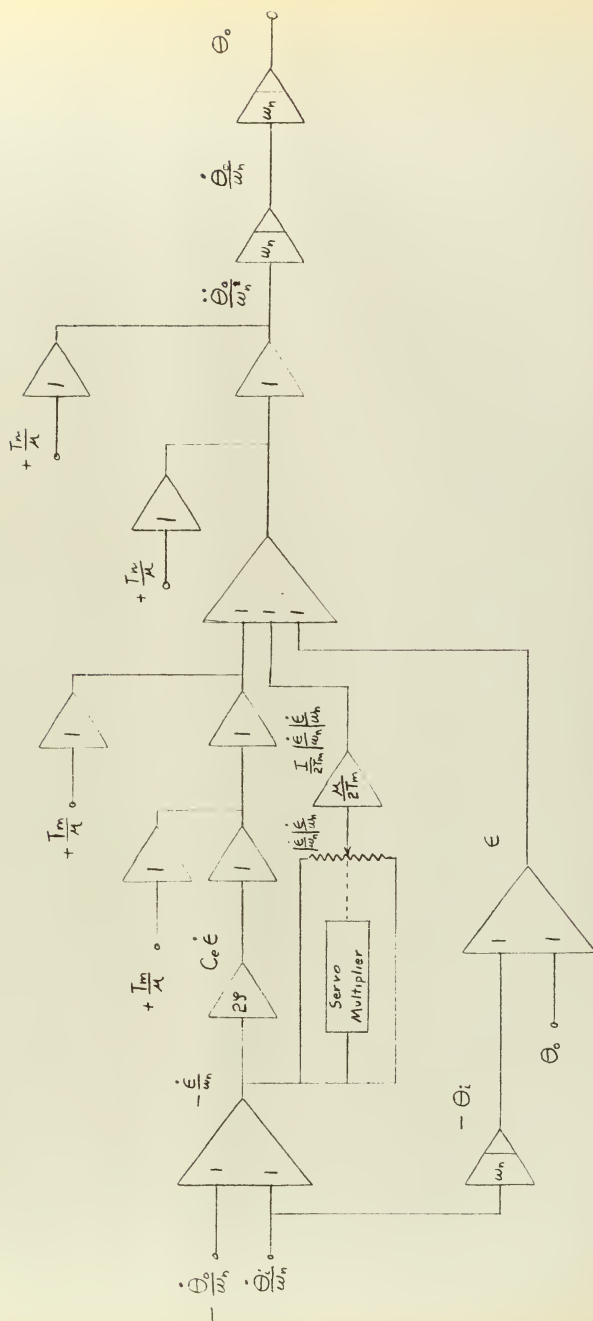


FIGURE 2 — Computer Circuit for a Frictionless Predictor Servo



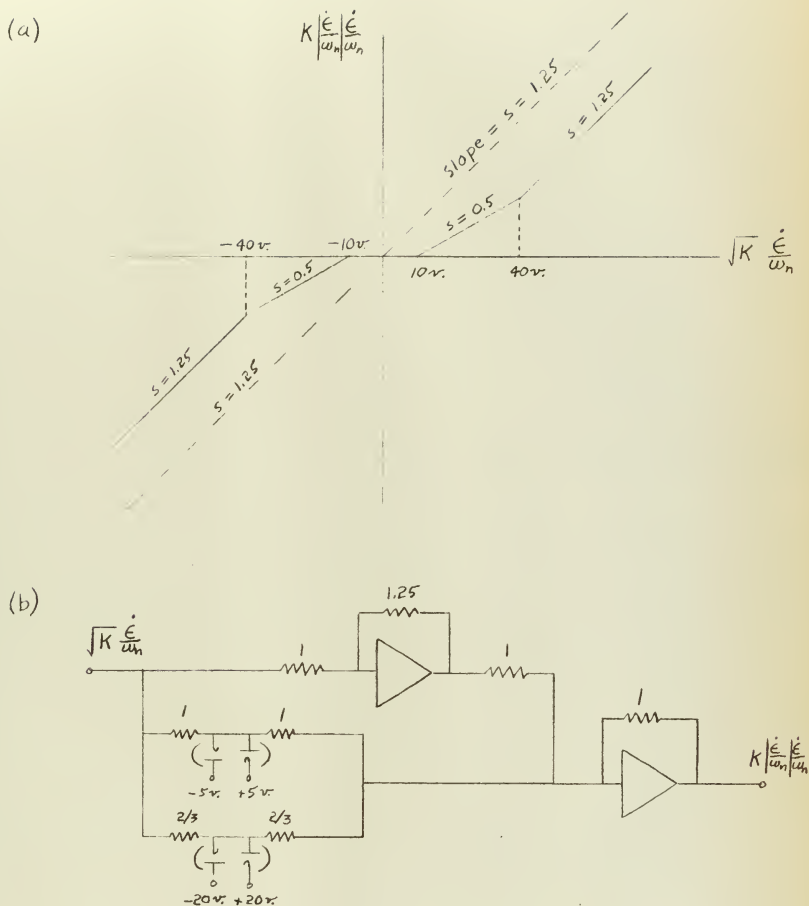


FIGURE 5 — (a) Approximate Prediction Curve for a Frictionless Servo, $K = \mu/2T_m$, and a Servo with Coulomb Friction, $K = \mu/2(T_m + C)$
 (b) Corresponding Diode Function Generator Circuit

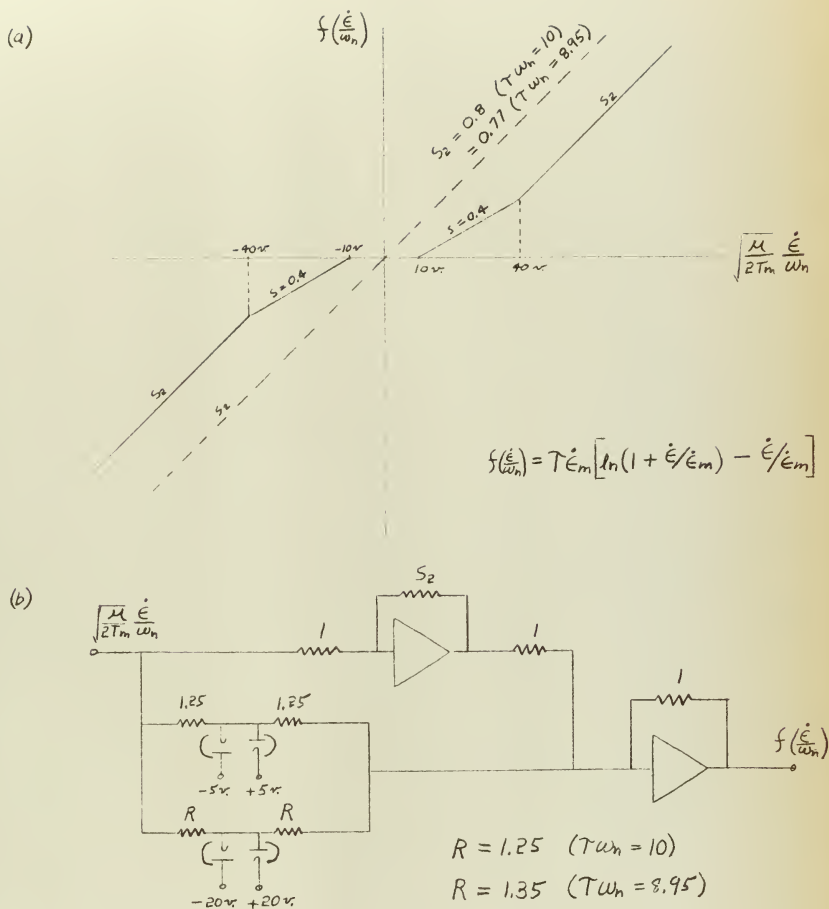


FIGURE 6 — (a) Approximate Prediction Curve for a Servo with Viscous Friction, $T\omega_n = 10, 8.95$
 (b) Corresponding Diode Function Generator Circuit

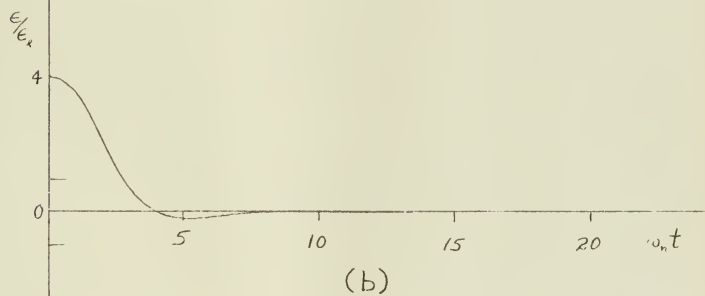
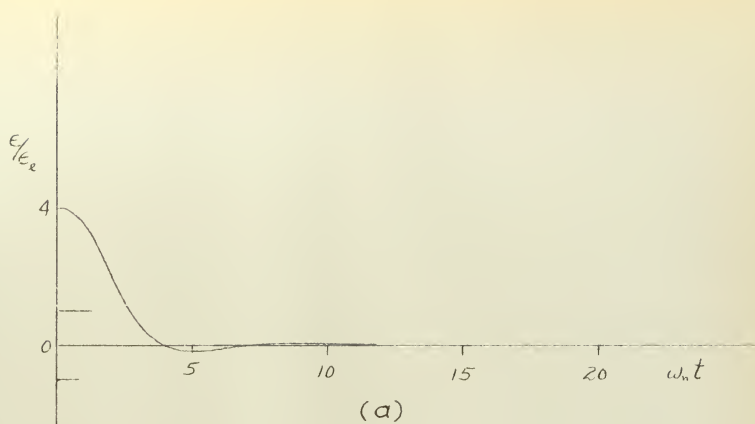


FIGURE 7 — Step Response of a Frictionless Servo with
Proportional and Error Rate Control, $C_e = 1/\omega_n$
(a) With Prediction (b) Without Prediction

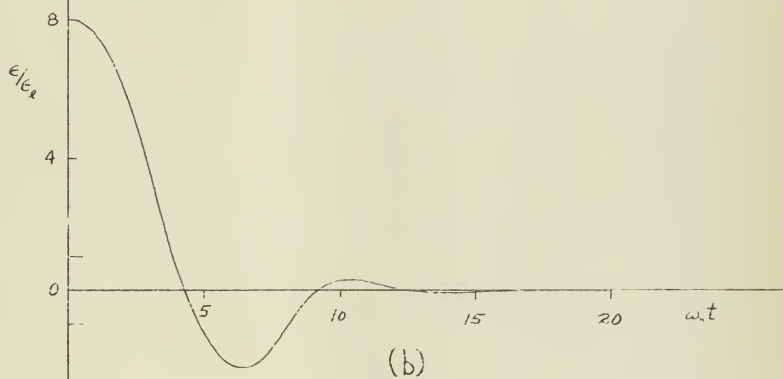
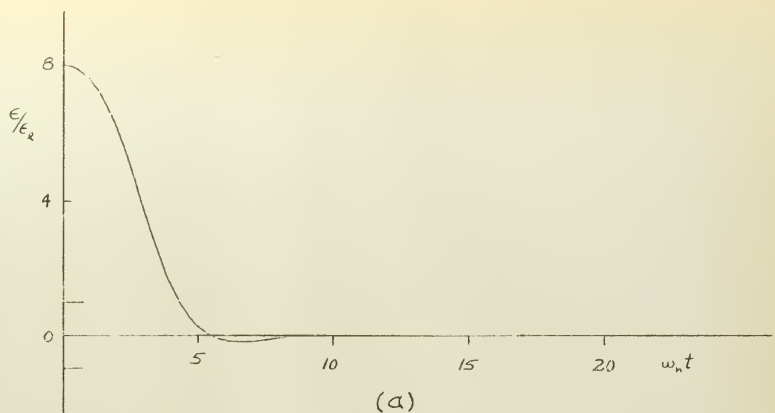


FIGURE 8 — Step Response of a Frictionless Servo with Proportional and Error Rate Control, $C_e = 1/\omega_n \eta$
 (a) With Prediction (b) Without Prediction

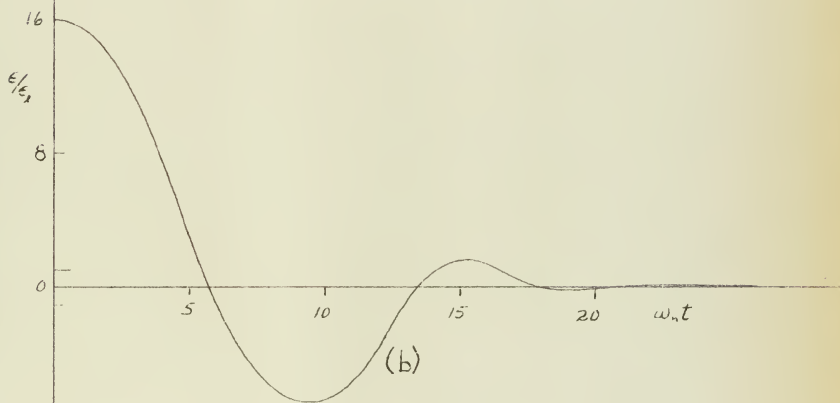
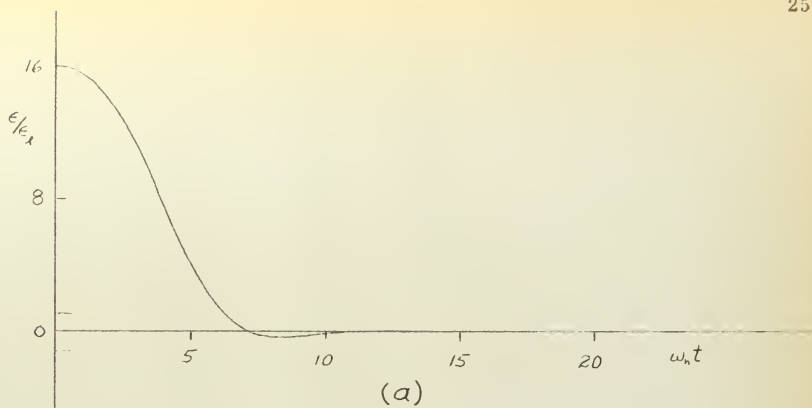


FIGURE 9 — Step Response of a Frictionless Servo with Proportional and Error Rate Control, $C_e = 1/\omega_n$

(a) With Prediction

(b) Without Prediction

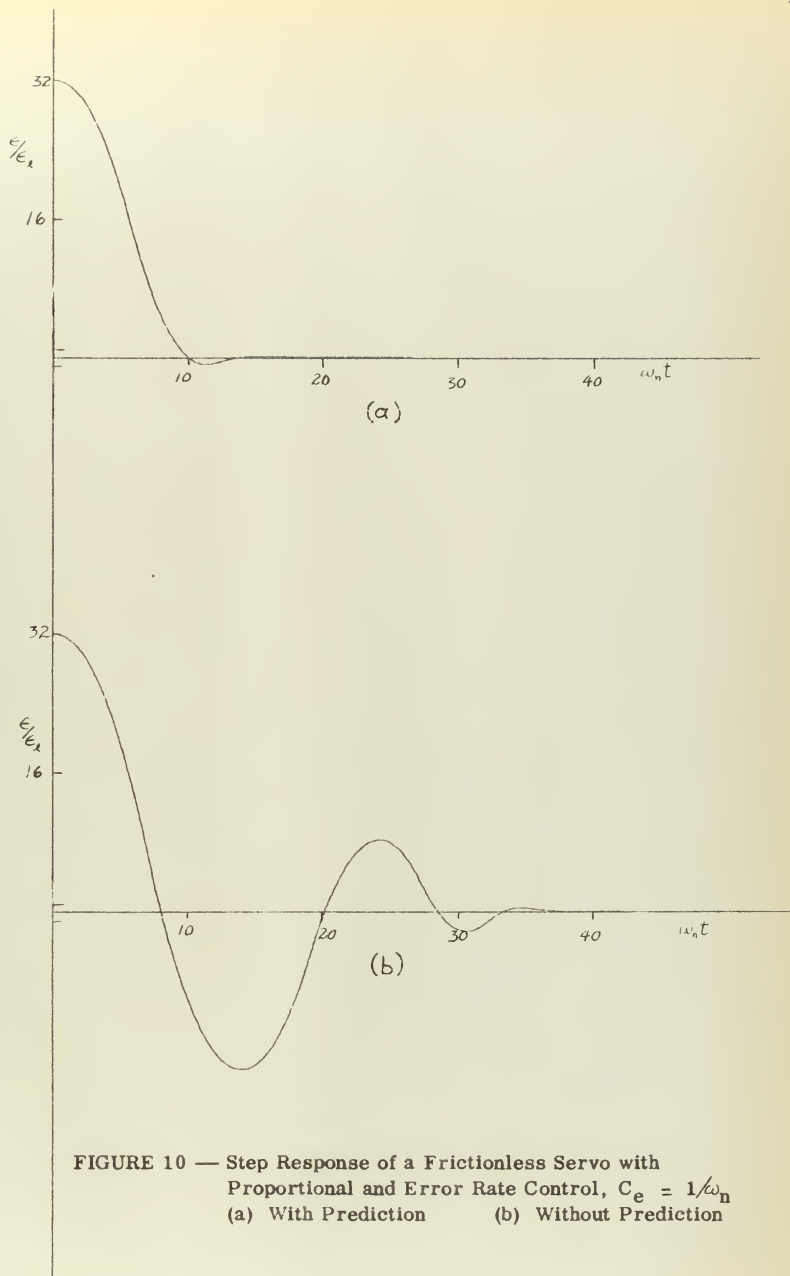


FIGURE 10 — Step Response of a Frictionless Servo with
Proportional and Error Rate Control, $C_e = 1/\omega_n$
(a) With Prediction (b) Without Prediction

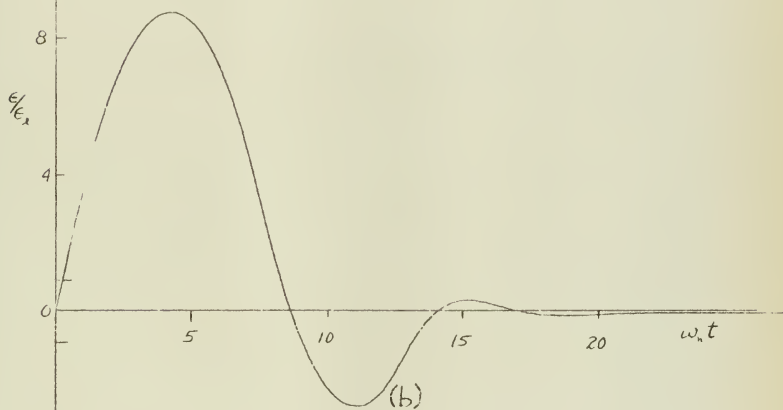
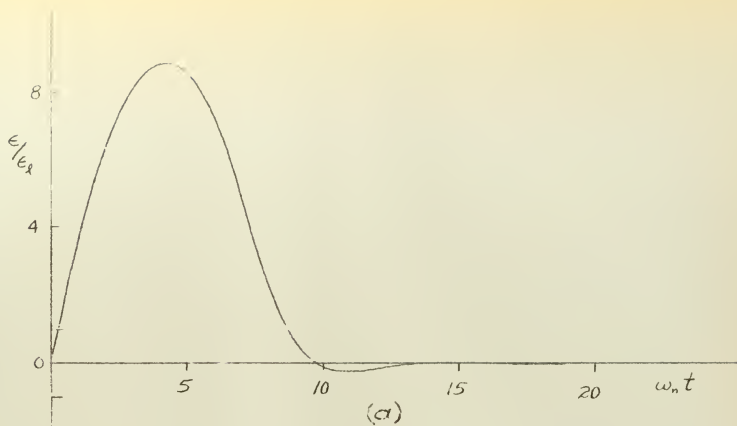


FIGURE 11 — Ramp Response of a Frictionless Servo with
Proportional and Error Rate Control, $C_e = 1/\omega_n$,
 $\theta_i/\omega_n = 0.1$
(a) With Prediction (b) Without Prediction

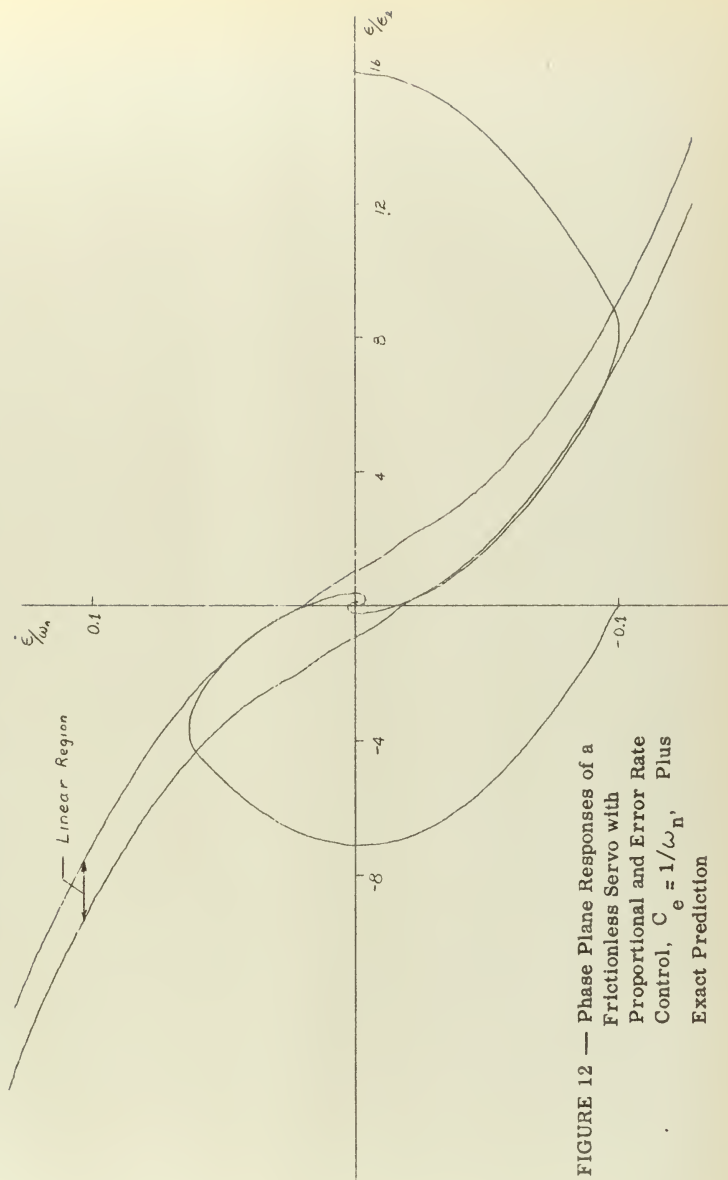


FIGURE 12 — Phase Plane Responses of a Frictionless Servo with Proportional and Error Rate Control, $C_e = 1/\omega_n$, Plus Exact Prediction

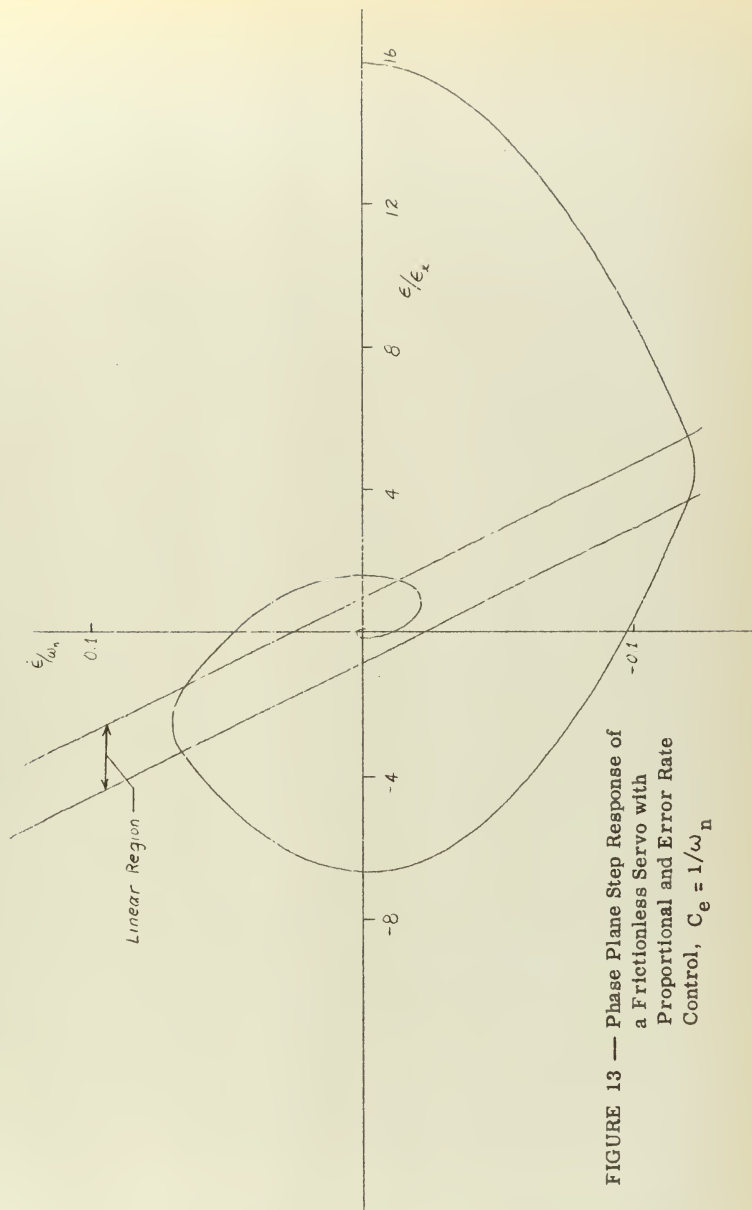


FIGURE 13 — Phase Plane Step Response of a Frictionless Servo with Proportional and Error Rate Control, $C_e = 1/\omega_n$

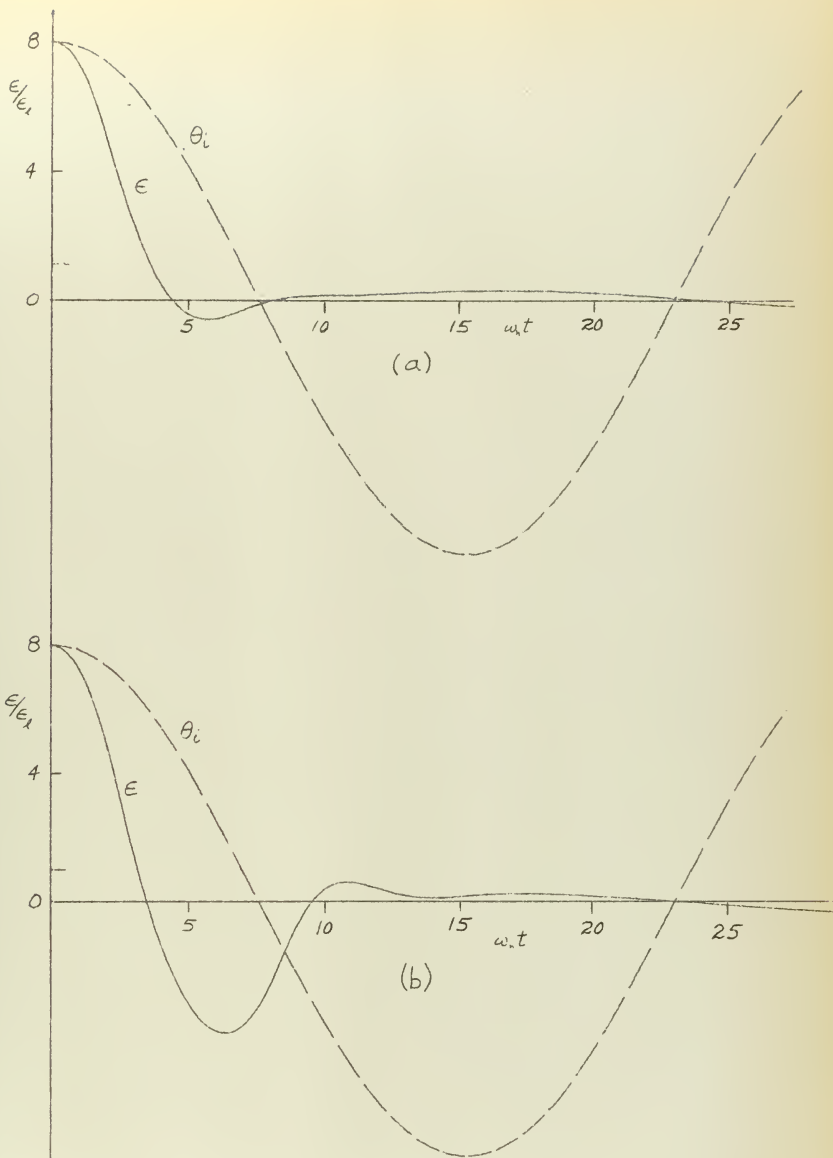


FIGURE 14 — Sine Wave Response of a Frictionless Servo with Proportional and Error Rate Control, $C_e = 1/\omega_n$.

$$\Omega/\omega_n = 1/5, \quad \ddot{\theta}_1(\max)/\dot{\theta}_0(\max) = 0.32$$

(a) With Prediction

(b) Without Prediction

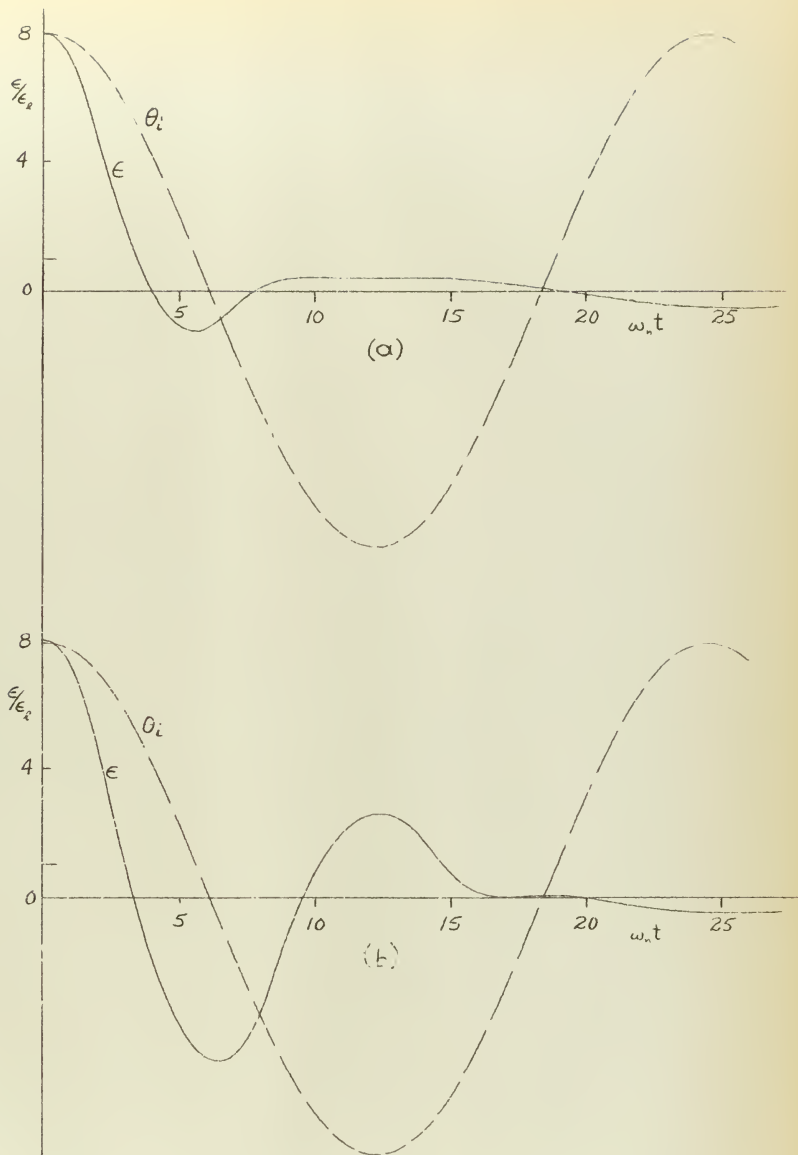


FIGURE 15 — Sine Wave Response of a Frictionless Servo with Proportional and Error Rate Control, $C_e = 1/\omega_n$, $\Omega/\omega_n = 1/4$, $\dot{\theta}_1(\max)/\theta_0(\max) = 1/2$
 (a) With Prediction (b) Without Prediction

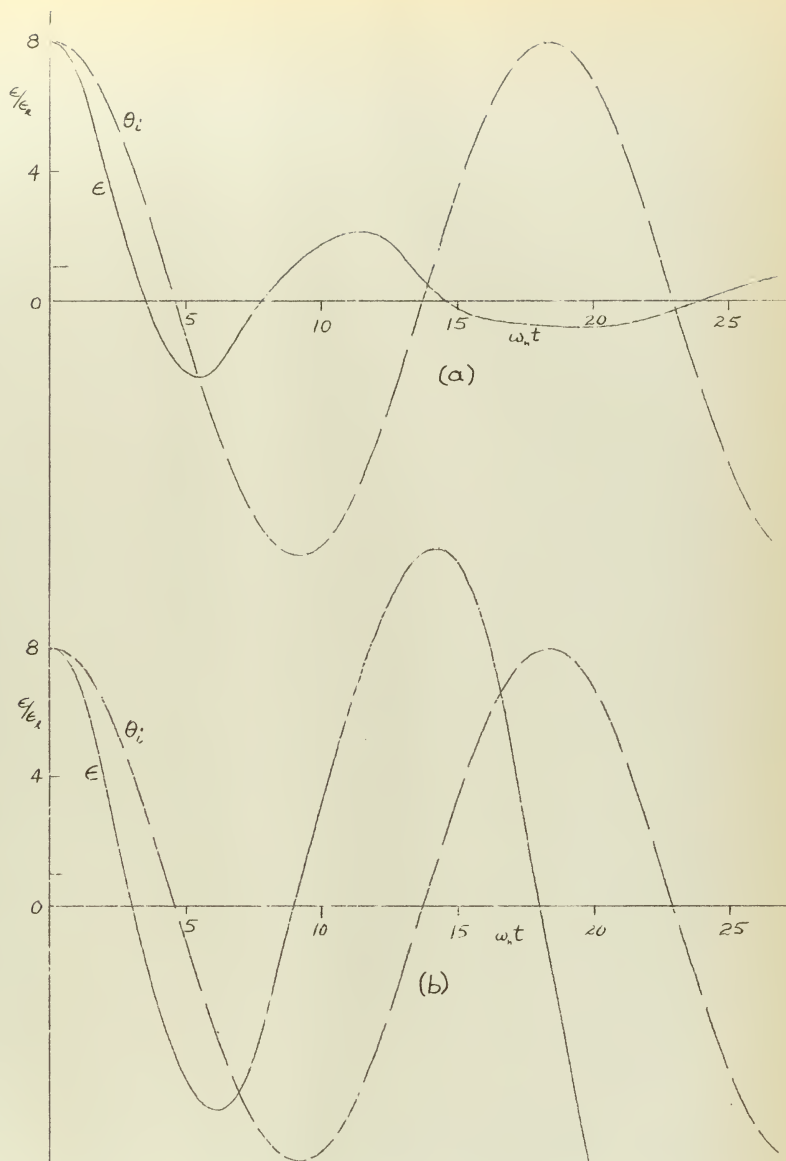


FIGURE 16 — Sine Wave Response of a Frictionless Servo with Proportional and Error Rate Control, $C_e = 1/\omega_n$, $\Omega/\omega_n = 1/3$, $\dot{\theta}_i(\max)/\dot{\theta}_o(\max) = 8/9$
 (a) With Prediction (b) Without Prediction

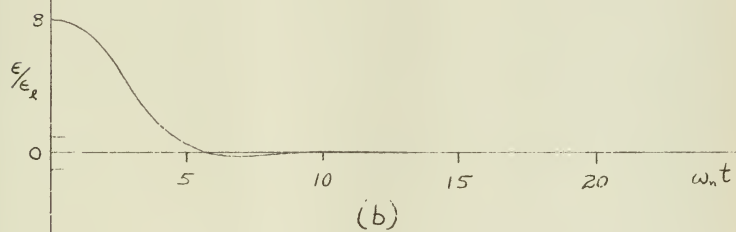
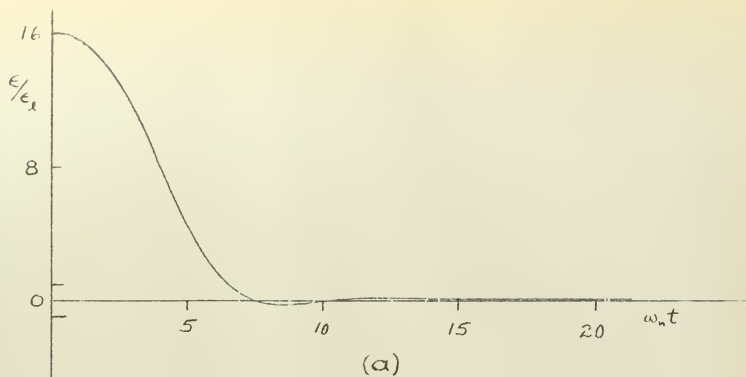


FIGURE 17 — Step Responses of a Frictionless Servo with Proportional and Error Rate Control, $C_e = 1/\omega_n$, Plus Approximate Prediction.

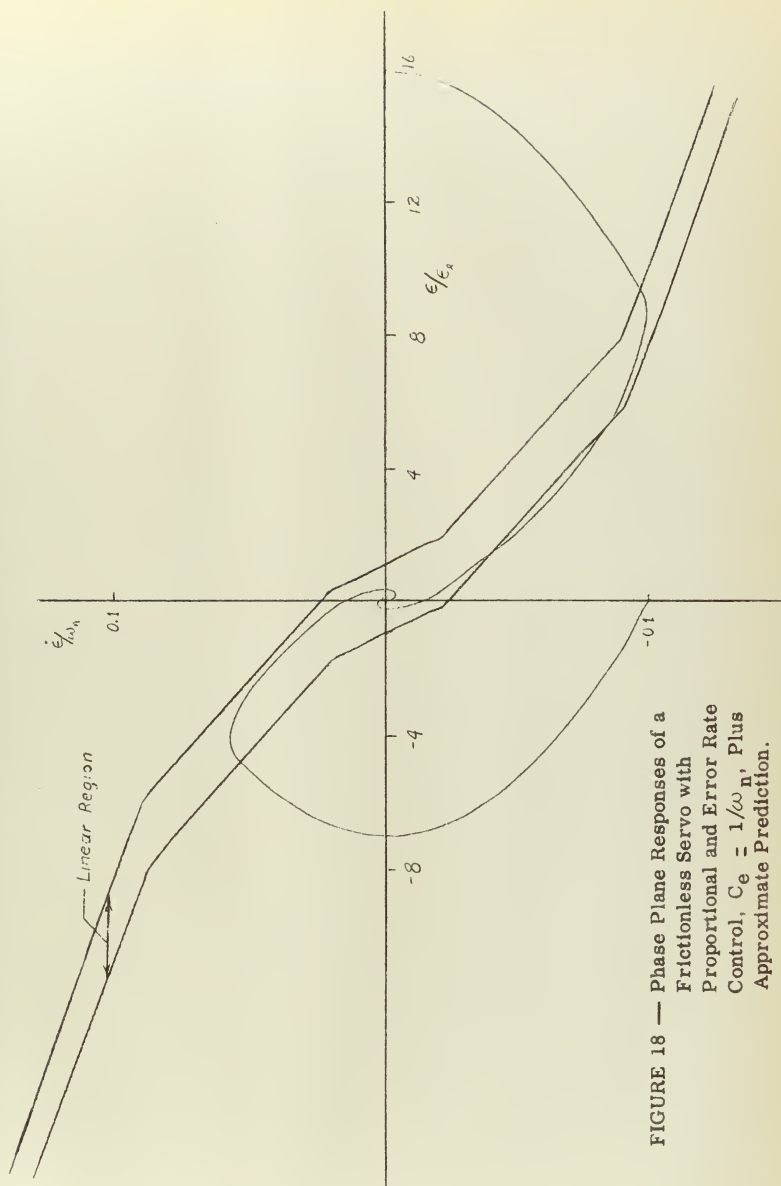


FIGURE 18 — Phase Plane Responses of a Frictionless Servo with Proportional and Error Rate Control, $C_e = 1/\omega_n$, Plus Approximate Prediction.

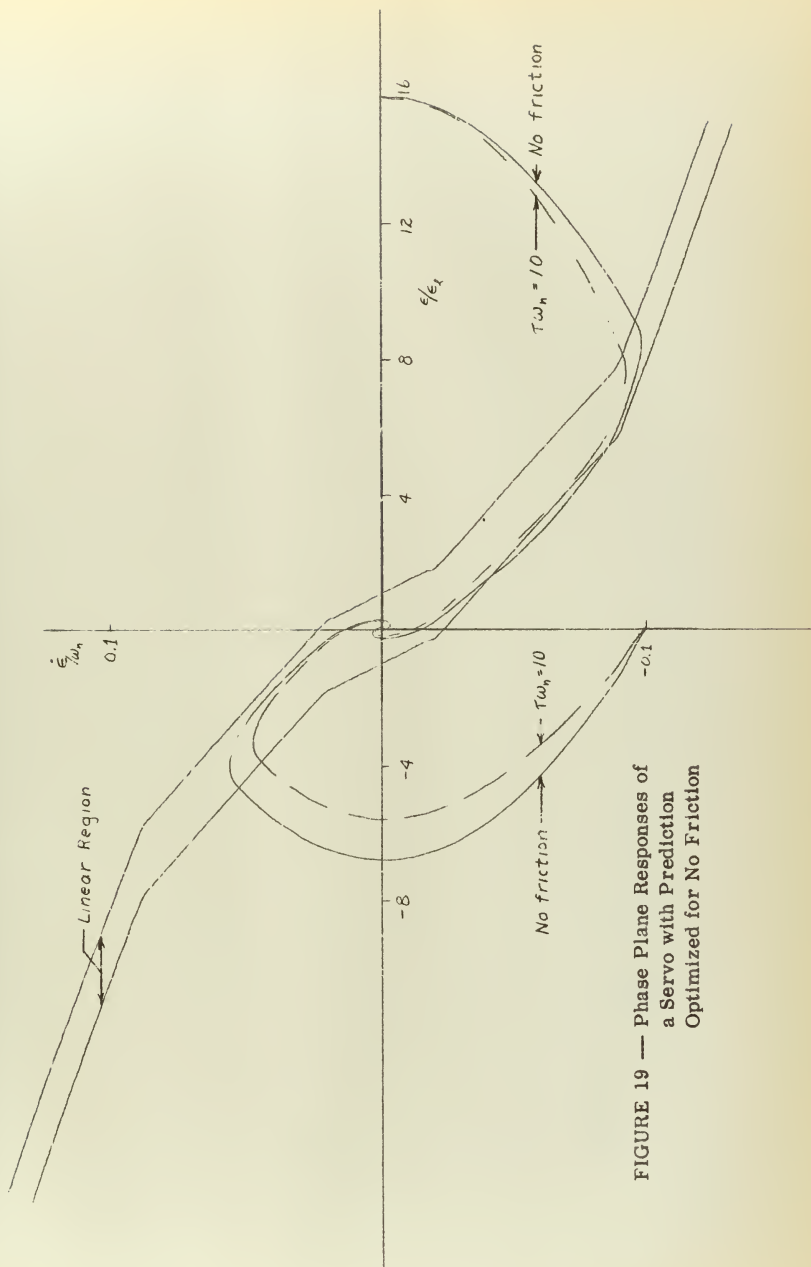


FIGURE 19 — Phase Plane Responses of a Servo with Prediction Optimized for No Friction

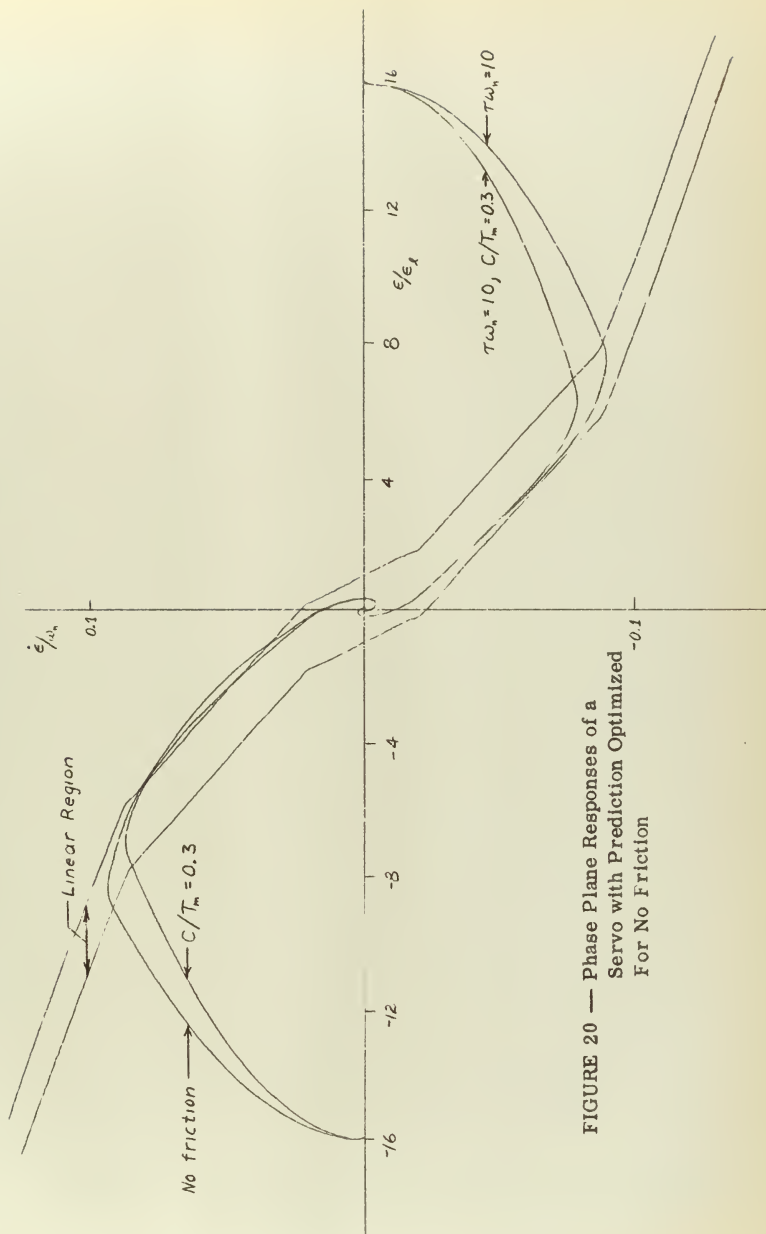


FIGURE 20 — Phase Plane Responses of a Servo with Prediction Optimized For No Friction

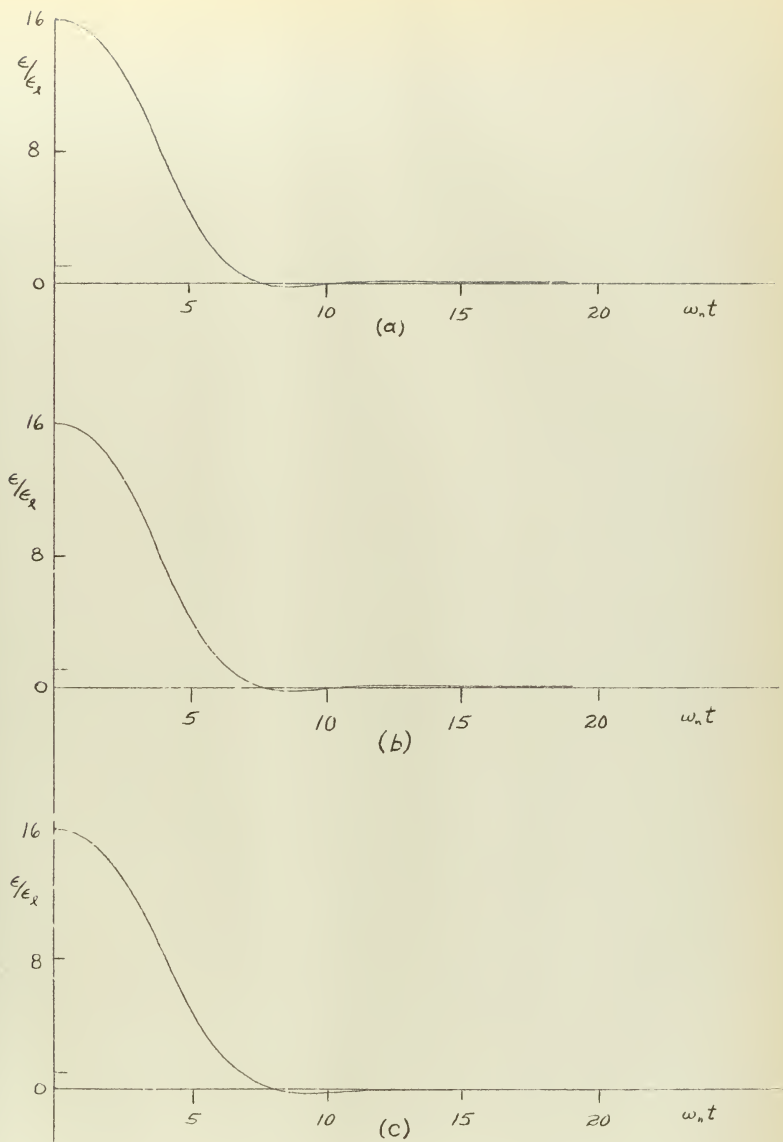


FIGURE 21 — Step Response of a Servo with Prediction Optimized for No Friction

(a) No Friction (b) $\tau\omega_n = 100$ (c) $\tau\omega_n = 10$

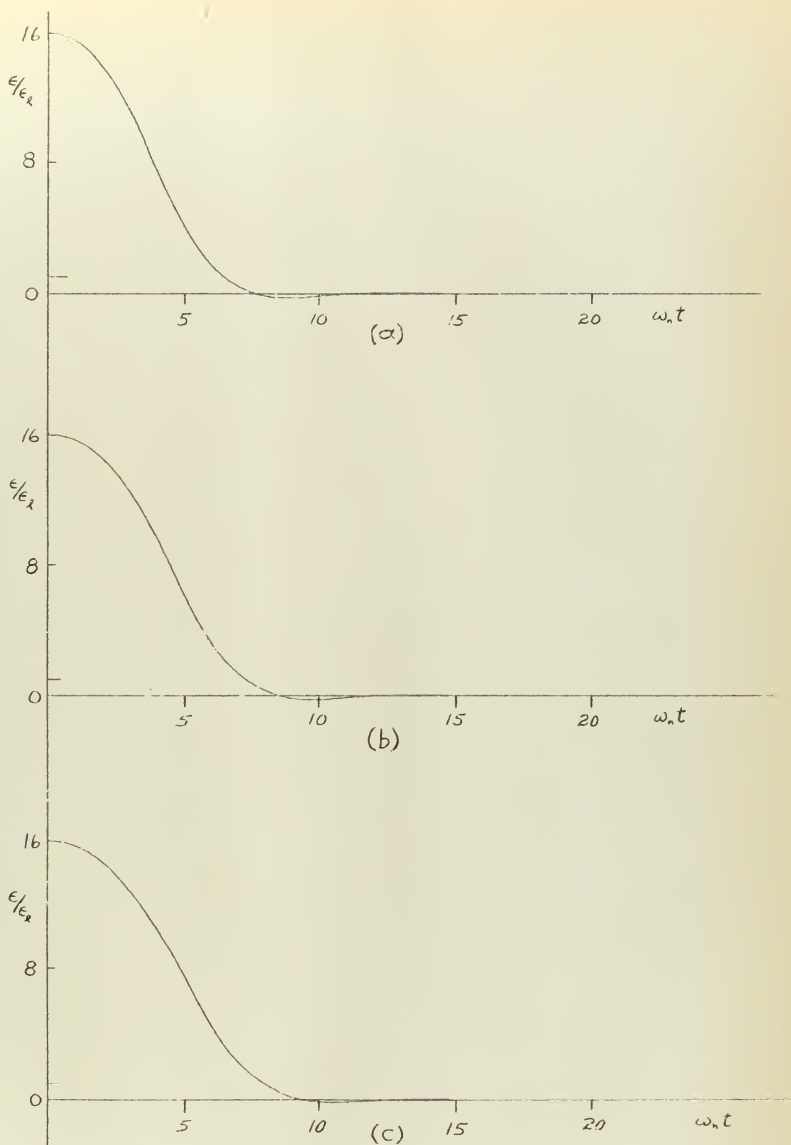


FIGURE 22 — Step Response of a Servo with Prediction Optimized
 for No Friction (a) No Friction (b) No Viscous
 Friction, $C/T_m = 0.3$ (c) $\tau\omega_n = 10$, $C/T_m = 0.3$

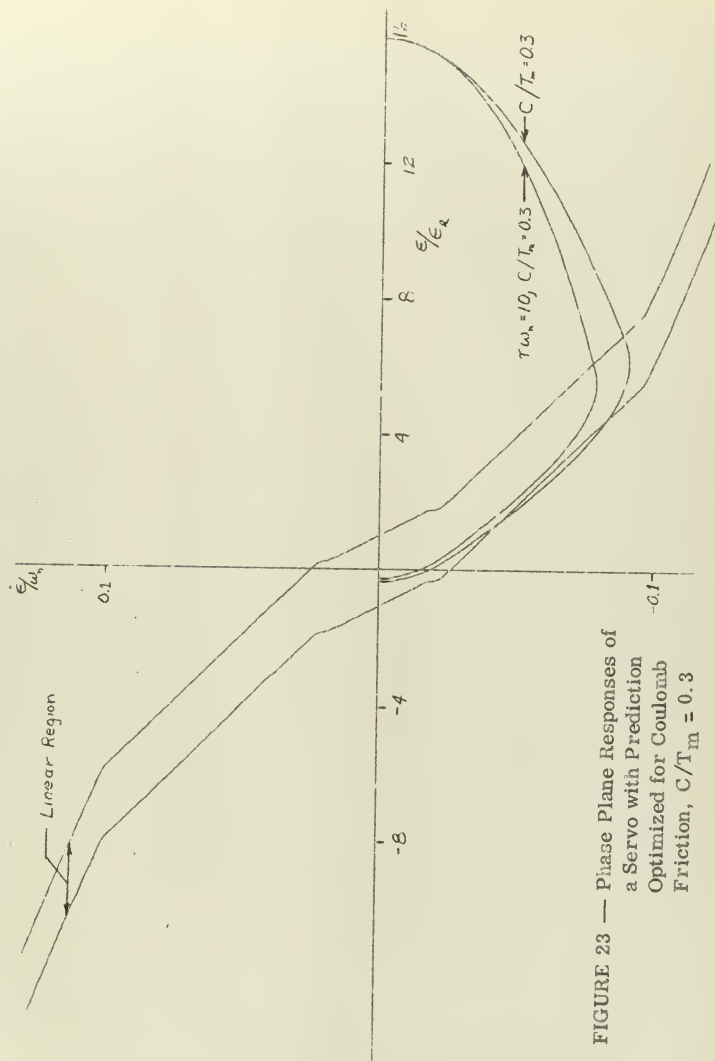


FIGURE 23 — Phase Plane Responses of a Servo with Prediction Optimized for Coulomb Friction, $C/T_m = 0.3$

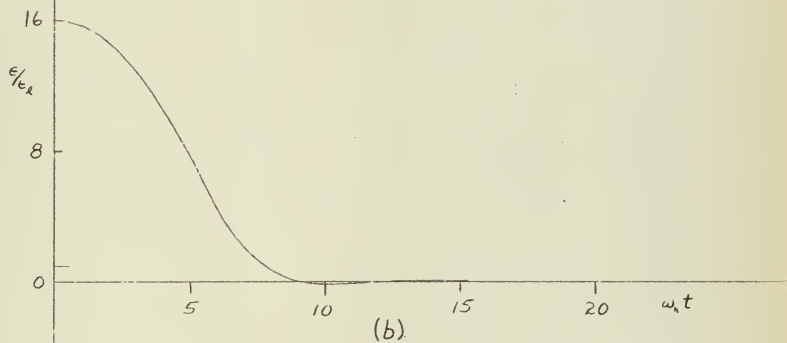
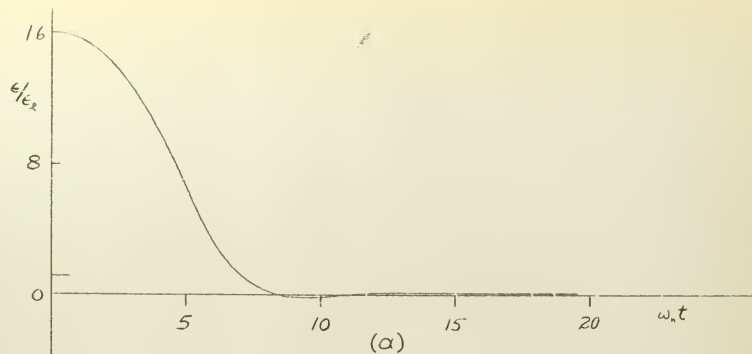


FIGURE 24 — Step Response of a Servo with Prediction
 Optimized for Coulomb Friction, $C/T_m = 0.3$
 (a) No Viscous Friction (b) $\tau\omega_n = 10$

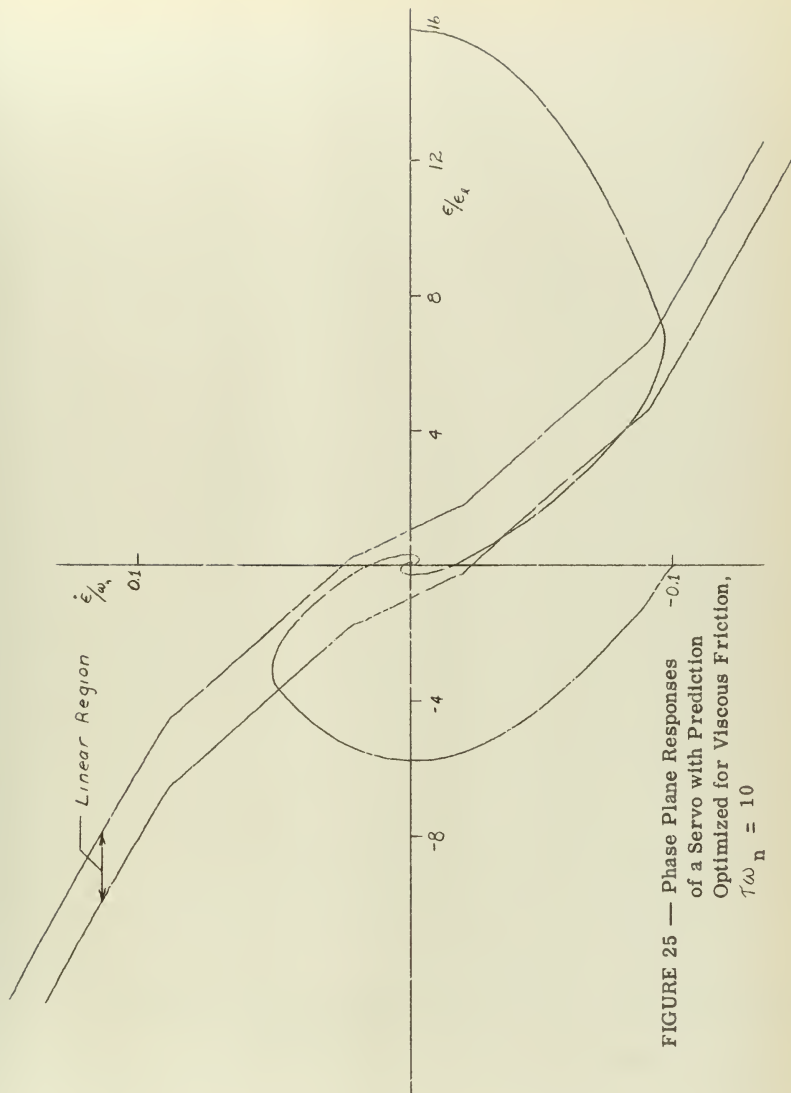


FIGURE 25 — Phase Plane Responses
of a Servo with Prediction
Optimized for Viscous Friction,
 $\tau\omega_n = 10$

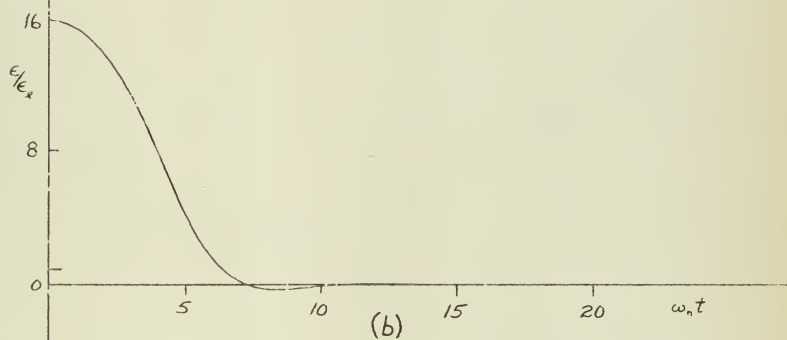
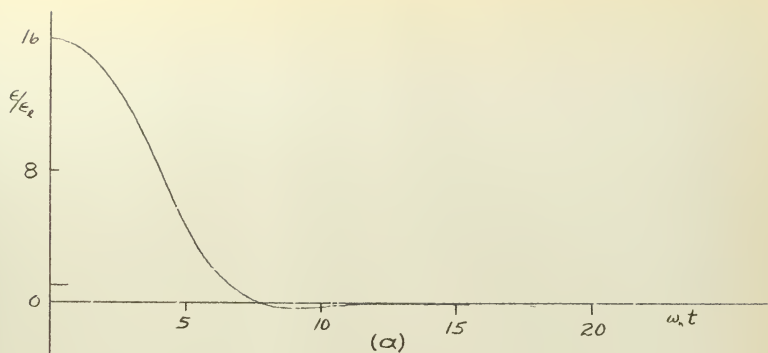


FIGURE 26 — Step Responses of a Servo, $\tau\omega_n = 10$, with Prediction Optimized for

(a) No Friction (b) Viscous Friction, $\tau\omega_n = 10$

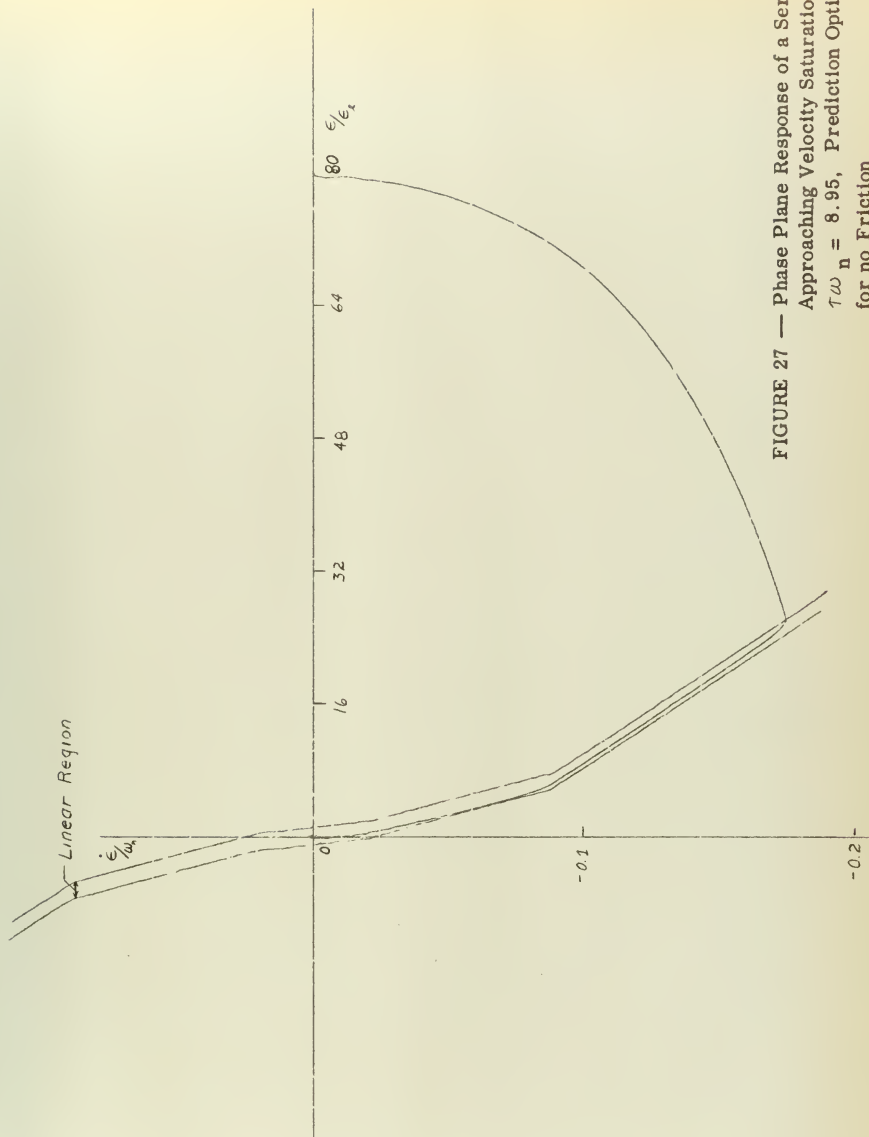


FIGURE 27 — Phase Plane Response of a Servo
Approaching Velocity Saturation,
 $\tau\omega_n = 8.95$, Prediction Optimized
for no Friction

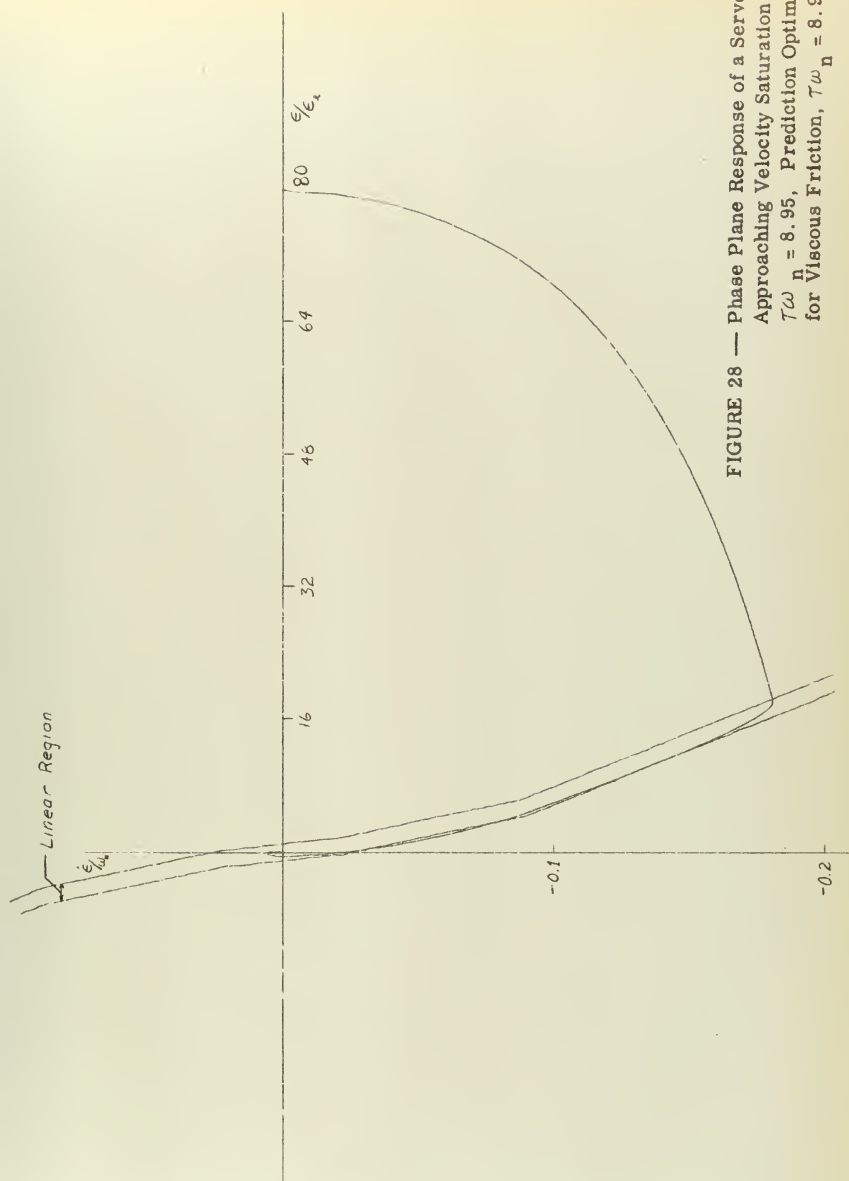


FIGURE 28 — Phase Plane Response of a Servo
Approaching Velocity Saturation,
 $\tau\omega_n = 8.95$, Prediction Optimized
for Viscous Friction, $\tau\omega_n = 8.95$

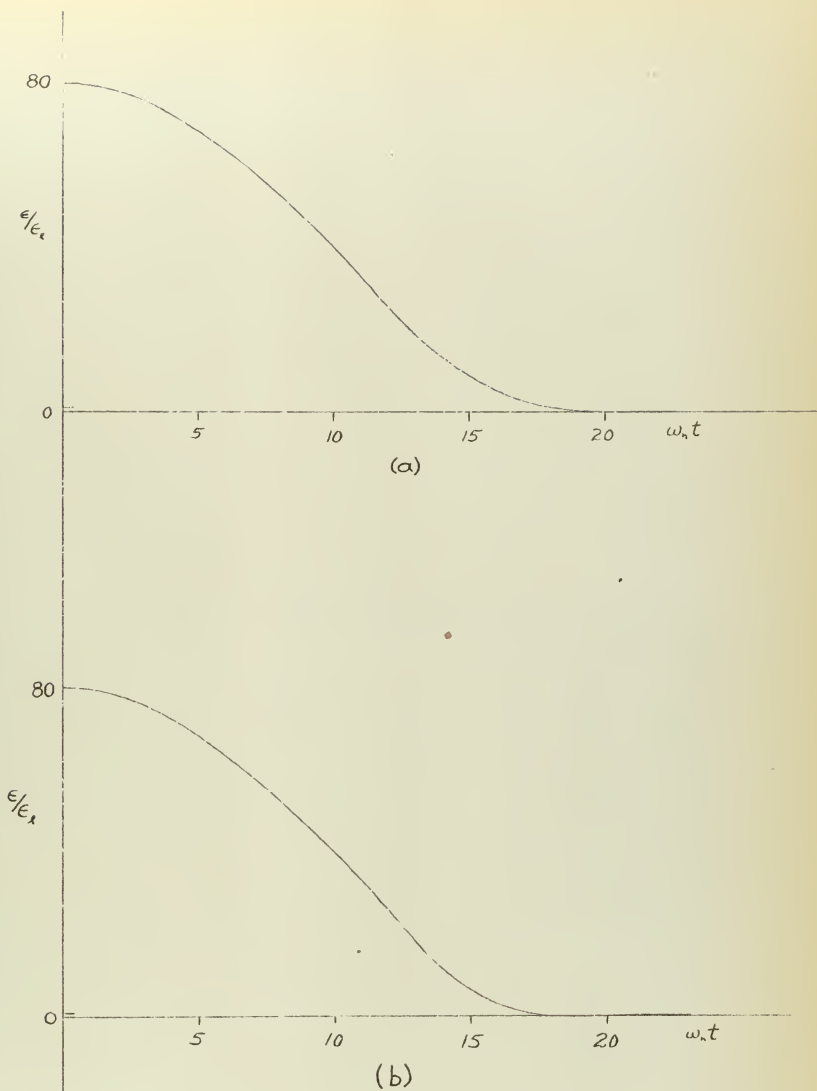


FIGURE 29 — Step Responses of a Servo Approaching Velocity
 Saturation, $\tau\omega_n = 8.95$, Prediction Optimized for
 (a) No Friction (b) Viscous Friction, $\tau\omega_n = 8.95$

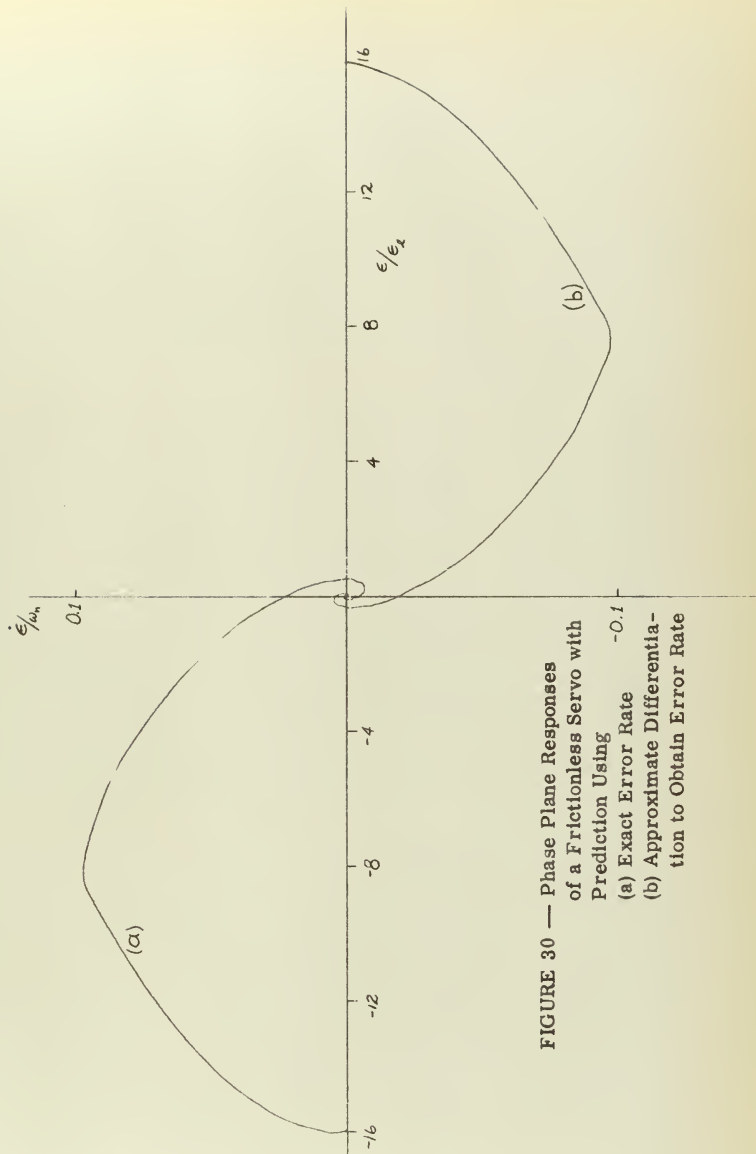


FIGURE 30 — Phase Plane Responses
of a Frictionless Servo with
Prediction Using
(a) Exact Error Rate
(b) Approximate Differential
Equation to Obtain Error Rate

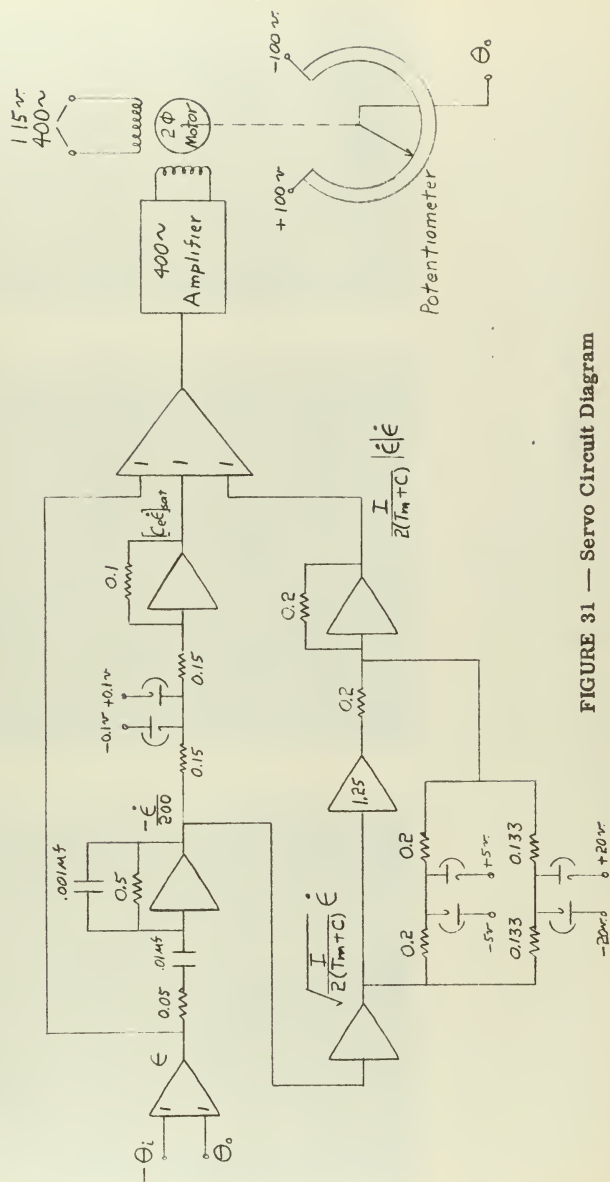


FIGURE 31 — Servo Circuit Diagram

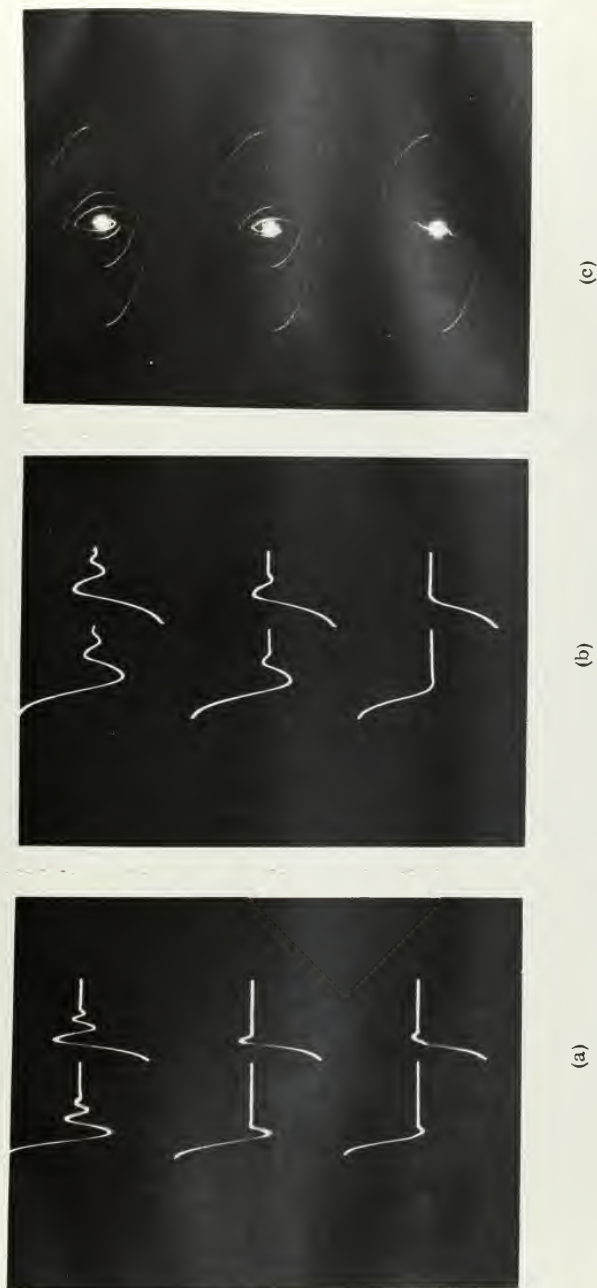


FIGURE 32

Responses of a Servo with Proportional Control (Top),
 Proportional Plus Error Rate Control (Center) and Prediction (Bottom)
 (a) 10 Volt Step (b) 100 Volt Step (c) Phase Plane for 100 Volt Step

REFERENCES

- (A) Rauch, L. L. and Howe, R. M., "A Servo With Linear Operation in a Region About the Optimum Discontinuous Switching Curve," Symposium on Nonlinear Circuit Analysis, April 25-27, 1956.
- (B) Lewis, J. B., "The Use of Nonlinear Feedback to Improve the Transient Response of a Servomechanism," Trans. AIEE, Vol. 71, Part 2, pp. 449-453, Oct., 1952.
- (C) McDonald, D., "Nonlinear Techniques for Improving Servo Performance," Proc. Natl. Electronics Conf., Vol. 6, pp. 400-421, 1950.
- (D) Silva, M., "Nonlinear Optimization of Relay Servomechanisms," Univ. of California, Inst. of Eng. Research, 1954.
- (E) McDonald, D., "Multiple Mode Operation of Servomechanisms," Rev. Sci. Instruments, Vol. 23, pp. 22-30, January, 1952.
- (F) Hopkin, A. M., "A Phase Plane Approach to the Compensation of Saturating Servomechanisms," AIEE Tech. Paper 51-103, 1951.

APPENDIX I

OPTIMUM SWITCHING CRITERIA

The minimum response time for a servo system with limited torque is obtained if the maximum available torque is applied to accelerate the system, and then the torque reversed for maximum deceleration to arrive simultaneously at zero error and zero error rate. If the torque is then removed, the error will remain zero until another command signal is given to the system. This type of response is discussed for three categories; a system with no friction, a system with only Coulomb friction, and a system with only viscous friction.

The problem of determining the exact time to reverse the torque depends in part upon the characteristics of the command signal. For the first two categories the acceleration of the command signal is assumed to be zero. That is, the switching time is optimized for constant or uniformly varying command signals. For the case with viscous friction, the switching time is optimized for a constant command signal.

First consider the system with no friction. The equation of motion is

$$I \ddot{\theta}_0 = \pm T_m = \text{torque}$$

or, in terms of error, since $\ddot{\theta}_1 = 0$,

$$\ddot{e} = \pm \frac{T_m}{I}$$

Integrating two times and assuming initial conditions of $\dot{e}(0) = 0$ and

$e(0) = 0$, the solution of the equation is

$$e = \pm \frac{T_m}{I} \frac{t^2}{2}$$

or

$$\epsilon = -\frac{1}{2T_m} \dot{\epsilon}^2$$

since $t = -\frac{1}{T_m} \dot{\epsilon}$ from the first integration.

In the phase plane of error and error rate, the solution paths are two parabolas passing through the origin as shown in Figure I-1.

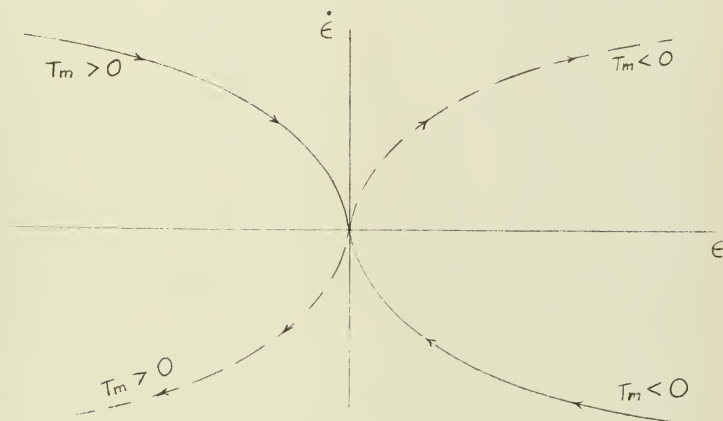


FIGURE I-1

Phase Plane Plot of Solutions Through the Origin

The parts of interest lie in the second and fourth quadrants, the other two portions represent divergent solutions. The phase plane is thus divided into two regions by the two segments of parabolas comprising the switching curve. The equation for this curve is

$$\epsilon = -\frac{1}{2T_m} |\dot{\epsilon}| \dot{\epsilon}$$

For a solution starting above and to the right of the switching curve, full positive torque applied will cause the solution to move along a parabolic path until it reaches the switching curve in the fourth quadrant. If the torque is then reversed, the response will follow the switching curve to the origin, and the torque can be reduced to zero. The same procedure applies to the other half of the phase plane with the opposite sense of torque. Sample phase plane trajectories are shown in Figure I-2.

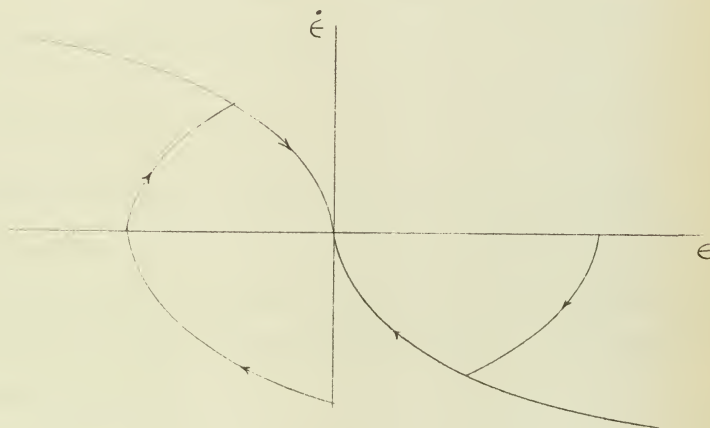


FIGURE I-2

Example Trajectories

Although this switching criterion represents the fastest response for large errors or error rates, a practical system mechanized in this manner would not follow slowly varying inputs smoothly due to switching delays and other non-ideal characteristics. A linear system with error rate or derivative feedback in addition to proportional control is better for this type of operation near the origin

in the phase plane. The torque in a linear system with proportional plus error rate control is proportional to $\epsilon + C_e \dot{\epsilon}$, and the optimum nonlinear system utilizes maximum torque tending to satisfy the equation

$$\epsilon + \frac{I}{2T_m} |\dot{\epsilon}| \dot{\epsilon} = 0$$

In combining the two systems, the torque should be made proportional to

$\epsilon + C_e \dot{\epsilon} + \frac{I}{2T_m} |\dot{\epsilon}| \dot{\epsilon}$. Near the origin of the phase plane, $\dot{\epsilon}$ is small and the term $\frac{I}{2T_m} |\dot{\epsilon}| \dot{\epsilon}$ is negligible compared to the others, hence the servo response is linear as desired. Away from the origin the $C_e \dot{\epsilon}$ term must be limited so the response will tend to make

$$\epsilon + \frac{I}{2T_m} |\dot{\epsilon}| \dot{\epsilon} = 0$$

For a large gain constant, μ , a small error, $\epsilon_x = T_m/\mu$, will torque saturate the system. If the $C_e \dot{\epsilon}$ term is made to saturate at a level exactly equal to the error required to torque saturate the servo, then away from the origin the response will lie exactly on the optimum switching curve. The equation of motion of the servo is then

$$I \ddot{\theta}_o = \mu \left[\epsilon + (C_e \dot{\epsilon})_{\text{sat} \pm \frac{T_m}{\mu}} + \frac{I}{2T_m} |\dot{\epsilon}| \dot{\epsilon} \right]_{\text{sat} \pm \frac{T_m}{\mu}}$$

where $\text{sat} \pm T_m/\mu$ represents the limits on the particular quantity in brackets.

In the phase plane, the torque equation represents a switching curve with a linear region adjacent to the switching curve. The limits of this linear region are shown in Figure I-3. The zero torque line lies midway between the boundaries of the linear region in the no friction case.

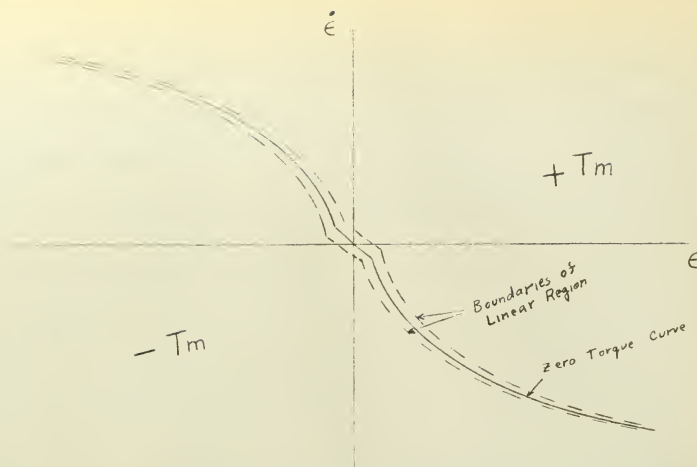


FIGURE I-3

Phase Plane Trajectory For the Optimum

Switching Curve with Linear Region

The extension of the above development to the case of a system with Coulomb friction is quite straightforward. The Coulomb friction represents a constant torque, C , which adds to servo torque during deceleration and subtracts from servo torque during acceleration. The switching curve equation then becomes

$$\epsilon + \frac{I}{2(T_m + C)} |\dot{\epsilon}| \dot{\epsilon} = 0$$

and the corresponding equation of motion of the system is

$$I\ddot{\theta}_o = \mu \left[\epsilon + (C_e \dot{\epsilon})_{\text{sat} \pm \frac{T_m}{\mu}} + \frac{I}{2(T_m + C)} |\dot{\epsilon}| \dot{\epsilon} \right]_{\text{sat} \pm \frac{T_m}{\mu}} \pm C$$

The effects of Coulomb friction on the switching curve are to increase the magnitude of the slope in a ratio $(1 + C/T_m)$, and to shift the zero torque line

from the center of the linear region.

In developing the equation of the switching curve for a system with viscous friction, the additional condition of $\dot{\theta}_i = 0$ was applied. The equation of motion of the system is now

$$I \ddot{\theta}_0 + f \dot{\theta}_0 = \text{torque} = \pm T_m$$

or in terms of error

$$\tau \ddot{e} + \dot{e} = \mp \dot{e}_m$$

where $\tau = I/f =$ time constant and $\dot{e}_m = T_m/f =$ maximum error rate

$$\dot{e} = \mp \dot{e}_m \left[1 - e^{-t/\tau} \right], \quad \dot{e}(0) = 0$$

or $t = -\tau \ln(1 \pm \dot{e}/\dot{e}_m)$

$$e = \mp \dot{e}_m \left[t - \tau (1 - e^{-t/\tau}) \right], \quad e(0) = 0$$

$$e = \pm \dot{e}_m \tau \left[\ln(1 \pm \dot{e}/\dot{e}_m) - \dot{e}/\dot{e}_m \right]$$

$$e + \tau \dot{e} = \tau \dot{e}_m \ln(1 + |\dot{e}/\dot{e}_m|), \quad \dot{e} > 0$$

$$e + \tau \dot{e} = -\tau \dot{e}_m \ln(1 + |\dot{e}/\dot{e}_m|), \quad \dot{e} < 0$$

The equation of motion of the servo system is then

$$I \ddot{\theta}_0 + f \dot{\theta}_0 = \mu \left[e + (C_\theta \dot{e})_{sat \pm \frac{T_m}{\mu}} \pm \tau \dot{e}_m \ln(1 + |\dot{e}/\dot{e}_m|) - \tau \dot{e} \right]_{sat \pm \frac{T_m}{\mu}}$$

To compare the switching curve for viscous friction to the one with no friction, consider for the moment, positive $\dot{\epsilon}$.

$$\text{Let } x = \sqrt{I/2T_m} \dot{\epsilon}$$

$$\text{and } m = \sqrt{2f^2/IT_m} = \sqrt{2/\tau} \dot{\epsilon}_m$$

The switching curve for no friction is

$$\epsilon = -\frac{I}{2T_m} \dot{\epsilon}^2 = -x^2$$

The switching curve for viscous friction is

$$\epsilon = \tau \dot{\epsilon}_m \left[\ln(1 + \dot{\epsilon}/\dot{\epsilon}_m) - \dot{\epsilon}/\dot{\epsilon}_m \right]$$

$$\epsilon = 2/m^2 \left[\ln(1 + mx) - mx \right]$$

Since $mx < 1$, expand $\ln(1 + mx)$ in a series

$$\epsilon = \frac{2}{m^2} \left\{ \left[mx - \frac{(mx)^2}{2} + \frac{(mx)^3}{3} - \frac{(mx)^4}{4} + \dots \right] - mx \right\}$$

$$\epsilon = \frac{2}{m^2} \left[-\frac{(mx)^2}{2} + \frac{(mx)^3}{3} - \frac{(mx)^4}{4} + \dots \right]$$

$$\epsilon = -x^2 \left[1 - \frac{2mx}{3} + \frac{(mx)^2}{2} - \frac{2(mx)^3}{5} + \dots \right]$$

It is apparent that for no friction, $m = 0$, the two curves are identical.

The difference is important only when mx is significant compared to 1. The same result can be obtained by comparing the slopes of the two curves.

$$\frac{d\epsilon}{dx} = -2x \quad \text{for } f = 0$$

and

$$\frac{d\epsilon}{dx} = \frac{-2x}{1 + mx} \quad \text{for } f \neq 0$$

Comparative curves are shown in Figure I-4 for several values of m .

The curves are terminated at $mx \leq 1$.

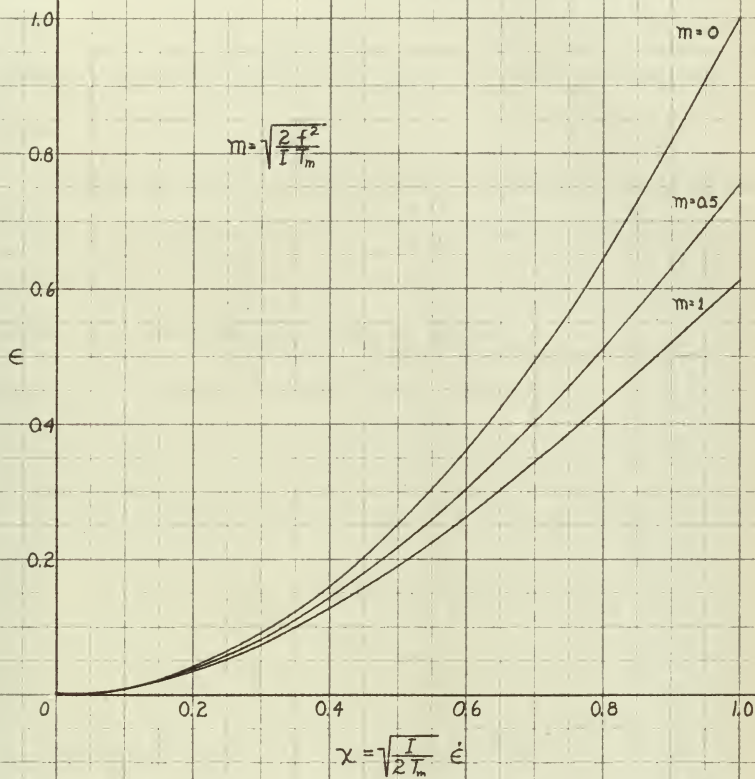


FIGURE I-4

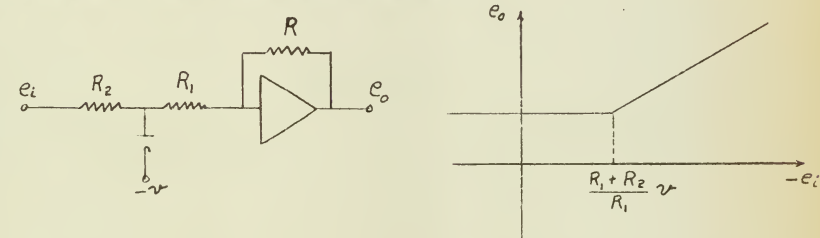
Switching Curves for Viscous Friction

APPENDIX II

THE FUNCTION GENERATOR

Any single valued function can be approximated by straight line segments to a reasonable degree of accuracy with an operational amplifier and biased diodes. The problem is only one of calculating the resistance values and bias voltages required to give the proper slope and location of the straight line segments.

Consider the circuit and response curve in Figure II-1. Make the assumption that the resistances are large compared to the grid to plate resistance of the diode and the power supply impedance so that the voltage drop across the conducting diode and in the power supply are negligible.



$$e_o = - \frac{R}{R_1} (-v)$$

$$e_i > - \frac{R_1 + R_2}{R_1} v$$

$$e_o = \frac{-R}{R_1 + R_2} e_i$$

$$e_i < - \frac{R_1 + R_2}{R_1} v$$

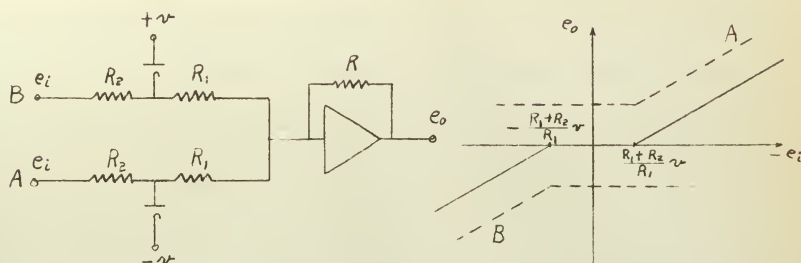
FIGURE II-1

(a) Diode Limiting Circuit

(b) Response Curve

If another input is now added with the diode reversed and biased positively, the output can be made symmetrical with respect to the origin. Symmetry is

not necessary, but is demonstrated below in Figure II-2 because of the particular function of interest in this report.



$$e_o = 0 \quad |e_i| < \frac{R_1 + R_2}{R_1} v$$

$$e_o = -\frac{R}{R_1} e_i \quad |e_i| > \frac{R_1 + R_2}{R_1} v$$

FIGURE II-2

(a) Symmetrical Diode
Limiting Circuit

(b) Response Curve

By adding other inputs with different resistances and bias voltages, more straight line segments can be generated and combined with the existing ones. Each input contributes a change in slope in the region where the diode is cut off, and a constant output elsewhere. Thus, by choosing the proper cut off voltage and resistance, the point of slope change and the amount of change are determined.

For most problems it is desirable to have a well defined, steady zero reference. If the diodes are conducting for zero input, drifting of the bias voltage, changes in the diode resistance and inequalities of resistances tend

to give output drift and balancing problems. For these reasons it is preferable to operate with the diodes cut off at zero input. This condition in general requires an additional operational amplifier if the second derivative of the function is positive, as it is in this servo problem. The procedure will be demonstrated for generation of the torque switching curve used for the frictionless servo.

It should be noted at this point that biased diodes could be used in the amplifier feedback circuit with an effect opposite to those in the input. This procedure was not used because it is difficult to generate a zero slope, and also a change of slope of any segment involves solution of a set of "n" simultaneous equations to determine the new resistance values where $(2n - 1)$ is the number of segments in the curve.

The mechanization of the switching curve involved generation of the functions,

$$\frac{I}{2T_m} \left| \dot{e} \right| \dot{e}, \text{ for the application to the servo, and the equivalent, } \frac{\mu}{2T_m} \left| \frac{\dot{e}}{\omega_n} \right| \frac{\dot{e}}{\omega_n}, \text{ for the simulation. In the first case } \dot{e} \text{ was multiplied by } \sqrt{I/2T_m} \text{ and in the second case } \dot{e}/\omega_n \text{ was multiplied by } \sqrt{\mu/2T_m}.$$

The multiplication conveniently scaled the input, e_i , and also reduced the problem to one of generating $|e_i| e_i$ for either case. The curve was approximated by five segments from $-100 < e_i < 100$ volts. This range corresponds to that from minus one to plus one in computer units. More segments were tried, but the change in performance of the servo was not noticeable.

The steepest slope was generated by one amplifier and the output of the other amplifier subtracted from it to generate the desired curve. The slopes used, range of input voltages, resistance, and bias voltages are tabulated below for positive e_i . The negative half of the curve is symmetric with respect to the origin. A one megohm feedback resistor is used.

TABLE II-1

Diode Function Parameters (No Friction)

e_i (volts)	Slope	Change of Slope	$R_1 = R_2$	Bias(Volts)
0 - 10	0	0	-	-
10 - 40	0.5	0.5	1.0	5
40 - 100	1.25	0.75	0.67	20

The resulting circuit appears in Figure II-3.

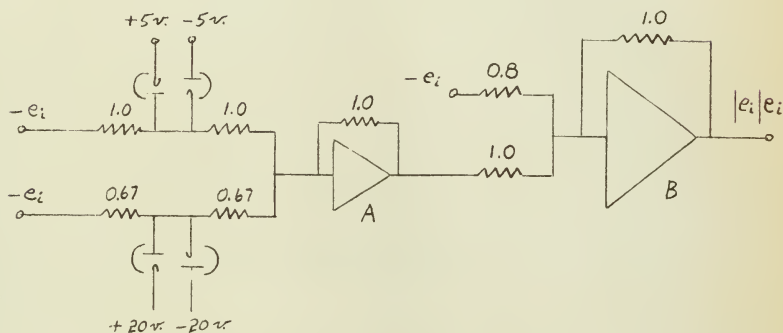


FIGURE II-3

Diode Function Generator (No Friction)

The outputs of the two amplifiers are shown below in Figure II-4 along with the contribution of the $-e_i$ input to amplifier B.

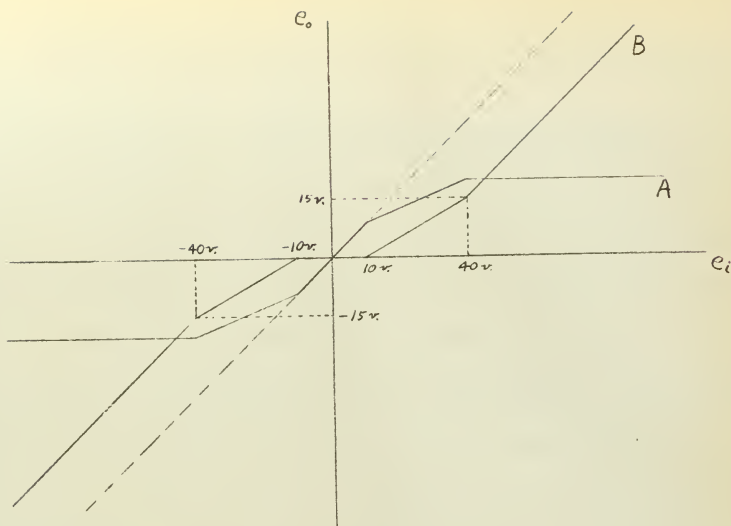


FIGURE II-4

Diode Function (No Friction)

Although this particular approximation appears very crude, a comparison of it to the true function shows there is no more than one volt error over half the range and four volts over 90% of the range.

By adding one more segment on each end, the error can be kept within one volt over 97.5% of full scale.

APPENDIX III

MAGNETIC AMPLIFIER CHARACTERISTICS AND COMPENSATION

To determine the static characteristics of the magnetic amplifier, a control current was supplied from an operational amplifier and the output terminals were connected to a 1320 ohm resistance load. This load represented ten watts at rated voltage. The static response curve is shown in Figure III-2.

The frequency response of the magnetic amplifier was obtained by again driving it from an operational amplifier with current feedback. The operational amplifier offered no bandwidth restrictions over the range of frequencies concerned. The frequency response curve in Figure III-3 shows that the output was down 3 db at about 17 cycles per second. By adding a 1.6 μ f condenser and 500 ohm resistor in parallel with the 10k resistor to ground, the output was kept quite flat out to about 200 cycles per second after which it falls off again. The control circuits are shown in Figure III-1.

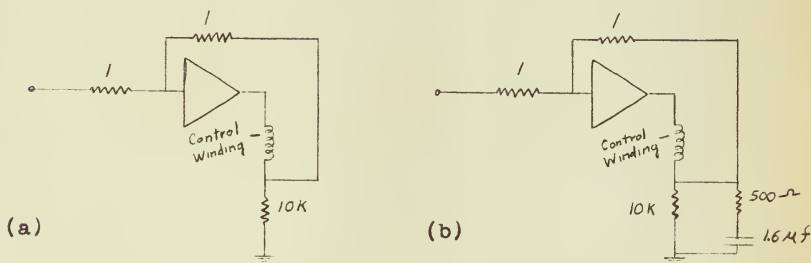


FIGURE III-1

Magnetic Amplifier Control Circuits

(a) Uncompensated (b) Compensated

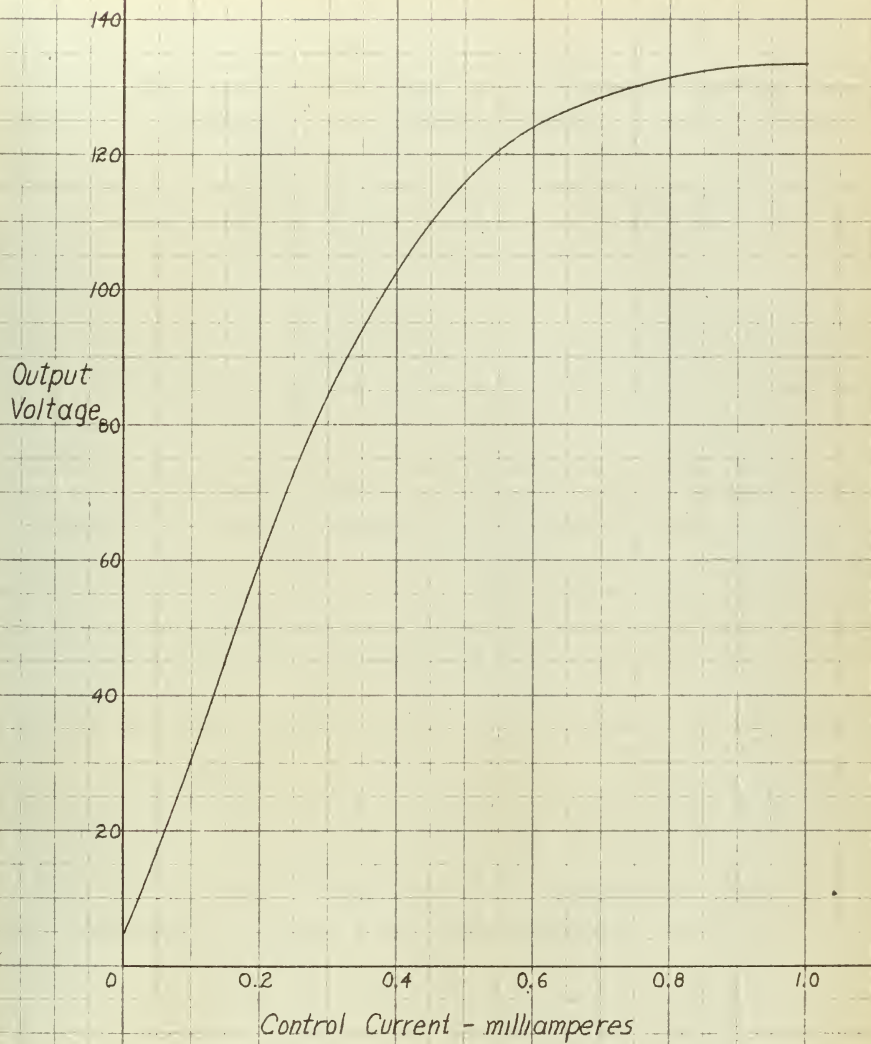


FIGURE III-2

Magnetic Amplifier Static Response

Compensated

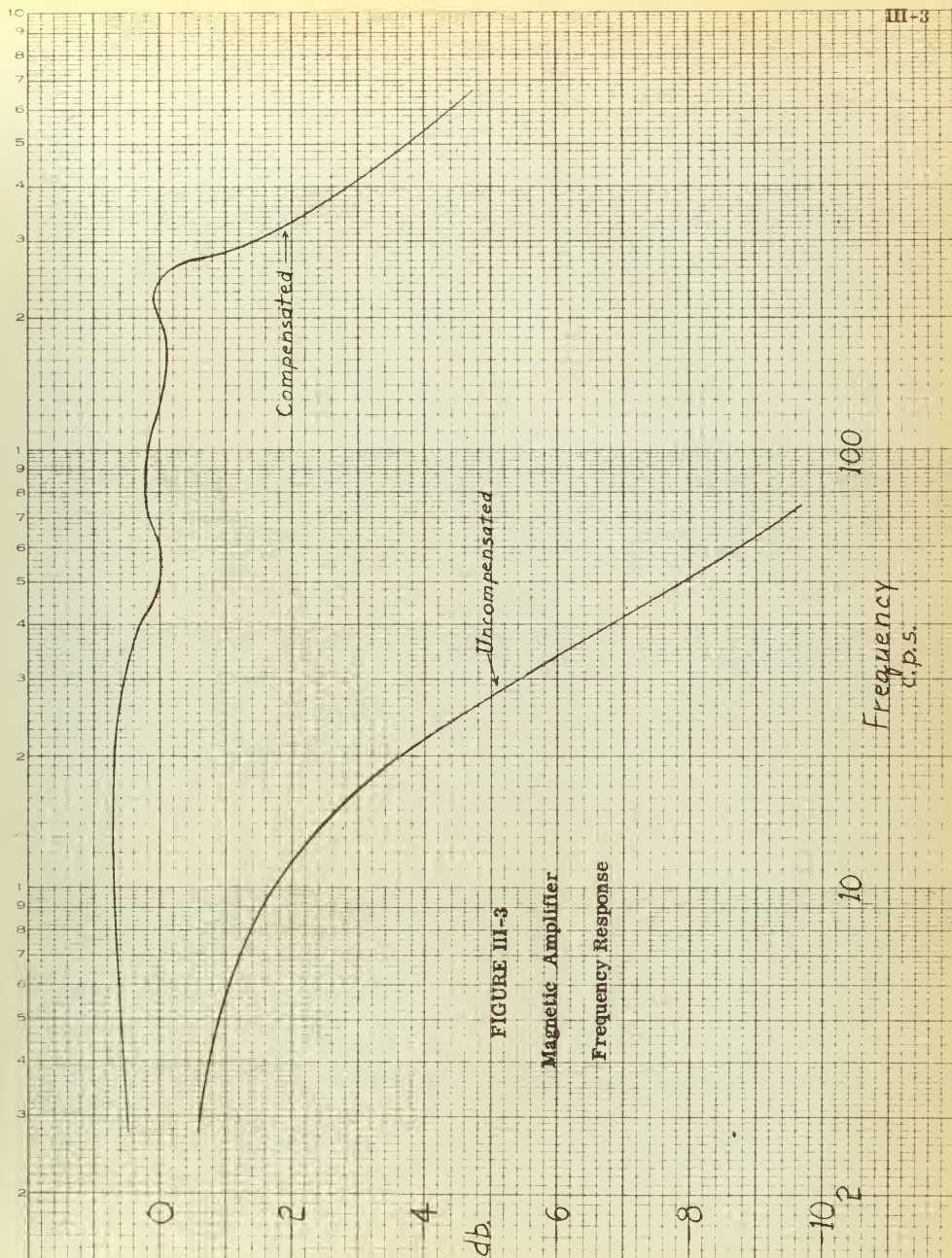
Uncompensated

Frequency
c.p.s.

FIGURE III-3

Magnetic Amplifier

Frequency Response



26 MAY 69

18222

Thesis
G255

Gay
Optimum prediction for
a torque saturating servo.

33143

26 MAY 69

18222

Thesis
G255

Gay

Optimum prediction for a
torque saturating servo.

33143

thesG255

Optimum prediction for a torque saturati



3 2768 002 02545 4

DUDLEY KNOX LIBRARY